

Second year progress review

Nicholas Harbour

Student ID: 14330088

ORCID: 0009-0008-2424-4516

Supervised by: Markus Owen and Matthew Hubbard

September 5, 2024

Centre for Mathematical Medicine and Biology, School of Mathematical Sciences,
University of Nottingham, Nottingham, NG7 2RD, UK

Table of contents

Preface	3
1 Summary	4
2 Literature review	6
2.1 Introduction	6
2.2 Stem cells in cancer	6
2.3 Cancer stem cells and treatment resistance	7
2.4 Mathematical models of cancer stem cell dynamics	8
2.4.1 Agent-based models	8
2.4.2 Integro-differential model	9
2.4.3 ODE model reduction	10
2.4.4 Stochastic model of CSC dynamics	12
2.4.5 A multispecies PDE model of cell lineages	13
2.5 Models of differentiation therapy	14
2.5.1 Differentiation promoter and self-renewal promoter	14
2.5.2 No self-renewal promoter	15
2.5.3 BMP4 in glioma	16
2.5.4 Summary of differentiation therapy results	16
2.6 Conclusion	17
3 Virtual Clinical Trials of BMP4 Differentiation Therapy: Digital Twins to Aid Glioblastoma Trial Design	18
3.1 Introduction	18
3.2 Materials and methods	20
3.2.1 Pre-clinical data	20
3.2.2 Model assumptions and equations	21
3.3 Results	24
3.3.1 Simulating radiotherapy experiments	24
3.3.2 Model simulations	26
3.3.3 Virtual clinical trial pipeline	27
3.4 Discussion	33
References	35

Preface

This is a Quarto book, to view it as HTML you can go here: <https://harbour-n.github.io/Second-year-report/>.

The report is structured as follows. In the first chapter I give a summary of the main results in my PhD over the first two years I then outline a brief plan for the remaining time of my PhD. In the second chapter I present a literature review specifically focusing on cancer stem cell modelling, the primary focus of my second year. In the third chapter I present our preprint [Virtual Clinical Trials of BMP4 Differentiation Therapy: Digital Twins to Aid Glioblastoma Trial Design](#), which will form a thesis chapter.

1 Summary

This chapter provides an overview of the progress in my PhD research and outlines the future direction of my thesis.

My PhD research centres on the mathematical modelling of cellular subpopulations in glioblastoma (GBM), the most common and aggressive primary malignant brain cancer in adults. During the first year, I focused on analysing single-cell and bulk RNA-seq data, aiming to extract dynamic information about tumour progression from these static snapshots, to motivate mathematical modelling. This lead to many conference talks/posters and a published abstract [Inference of cell cycle regulation between glioblastoma subpopulations *in vivo* to drive computational and mathematical models of the cancer complex system](#) from the Society of Neuro-Oncology annual meeting, although it may not form a significant part of my thesis.

Following my initial visit to the Mathematical Neuro-Oncology Lab, run by Kristin Swanson at the Mayo Clinic in May 2023, I became involved in a project investigating differentiation therapy as a novel treatment for GBM, this is a joint project with Dr Quinones lab in the department of Neurosurgery (Mayo Clinic Florida). This has become the primary focus of my second year. GBM remains almost universally fatal, partly due to its resistance to radiation therapy. Research has identified a subpopulation of cancer cells in GBM (and other cancers) with stem cell-like properties that make them highly resistant to conventional cytotoxic treatments, such as radiotherapy and chemotherapy. These cancer stem cells (CSCs), or glioma stem cells (GSC) in the case of glioma, are believed to drive tumour initiation, growth, and recurrence, making their eradication crucial for effective treatment. Dr Quinones' lab is developing new therapies for GBM using novel delivery mechanisms that aim to create a less favourable microenvironment for GBM to survive. One therapy they are particularly interested in is BMP4; this is a protein that has been shown to drive differentiation of GSCs towards a predominantly glial (astrocytic) fate, to reduce GBM tumor burden *in vivo* and to improve survival in a mouse model of GBM. Throughout my second year, we have been developing a mathematical model that simulates GSC-driven tumor growth in GBM, its response to BMP4 therapy and standard radiotherapy. Using data from five glioma stem cell lines provided by Dr. Quinones' lab, we have parameterized this model, enabling us to estimate the sensitivity of these cell lines to BMP4. We explore the model for a range of different parameters developing a virtual clinical trial approach to see how BMP4 impacts simulated GBM growth across a range of virtual cohorts. Our findings suggest that tumour proliferation rate is also a critical factor that must be accounted for when assessing BMP4 efficacy. Additionally, we have used this model to explore various BMP4 treatment schedules, with the ultimate goal of informing future clinical trial design.

In addition to this primary project, I have been involved in several other initiatives during my second year, which are not detailed anywhere else in this report. In November 2023 I took part in the Integrated Mathematical Oncology (IMO) workshop at the Moffit Cancer Center, Florida. Our team developed a mathematical model for evolutionary steering in breast cancer, came second place and won a pilot fund of \$50,000 to further this research project (<https://imoworkshop.org/IMO11/index.html>). In March 2024,

I undertook a second visit to the Mathematical Neuro-Oncology Lab at Mayo Clinic Arizona. During this visit I took part in an academic retreat focusing on sex differences and the the immune landscape in GBM. This visit strengthened my collaboration with the group, resulting in an official research internship position. From May to June I led a team of PhD students and research staff in a [datathon](#) run by the University of Exeter and EPSRC Hub for Quantitative Modelling in Healthcare. The goal was to quantify heterogeneity in human daily rhythms using time series data of hormone concentrations in healthy individuals. Our team won the prize for best negative result, using functional data analysis and machine learning techniques to demonstrate that circadian rhythm signals from sleep-wake cycles dominate over other signals that could differentiate patient metadata such as sex, age or weight.

The plan for my thesis includes several chapters based on a series of papers, a draft of the anticipated structure is as follows:

- **Introduction:** A short text explaining the context and structure of the thesis.
- **Outreach paper:** We aim to publish a paper in *Frontiers for Young Minds*, a journal targeting a young audience (ages 9-15). This could serve as an engaging and non-traditional introductory chapter to my thesis, explaining the basics of modelling in GBM.
- **Literature review:** An overall literature review, encompassing all of my work. This will be slightly broader than the literature review presented in this report (Chapter 2) that focuses specifically on the cancer stem cell literature that is particularly useful for understanding the context for my preprint.
- **BMP4 Virtual Clinical Trials:** This will be based on the preprint [Virtual Clinical Trials of BMP4 Differentiation Therapy: Digital Twins to Aid Glioblastoma Trial Design](#). We plan to submit this to a broad interdisciplinary science journal, focusing on the integration of data and modelling, as well as model-informed clinical trial design.
- **Mathematical Analysis of the model:** Following on from this we are planing on writing a paper that will consider the model from a more mathematical perspective. We have already begun some of this analysis such as steady states of the model, nullclines, model reductions, although this analysis is not included in this report.
- **Digital Twins and Alan Turing Institute:** Beginning in January 2025, I will participate in the Alan Turing Institute's PhD enrichment placement, which is designed to help PhD students deepen their research in machine learning and data science. The Institute hosts a center dedicated to digital twin research, where I plan to tackle some of the fundamental challenges in developing digital twins for healthcare, such as creating robust, uncertainty-aware models that can be effectively used in clinical settings. In collaboration with the Mathematical Neuro-Oncology Lab, we will apply these ideas to digital twin models for GBM.
- **Conclusion:** Drawing together the strands of the thesis.

2 Literature review

In this chapter we present a brief literature review particularly focused of stem cells in cancer and the different modelling approaches that have been used.

2.1 Introduction

Stem cells are defined as cells that have the ability to perpetuate themselves through self-renewal and to generate mature cells of a particular tissue through differentiation (Reya et al. 2001). Stem cells are fundamental to tissue maintenance and repair; they also play a critical role in cancer development and in determining the outcomes of cancer treatment (Weiss, Komarova, and Rodriguez-Brenes 2017).

2.2 Stem cells in cancer

Perhaps the most important and useful property of stem cells is that of self-renewal. Self-renewal is crucial to stem cell function, because it is required by the majority of stem cells to persist for the lifetime of the animal. Moreover, whereas stem cells from different organs may vary in their developmental potential, all stem cells must self-renew and regulate the relative balance between self-renewal and differentiation. Understanding the regulation of normal stem cell self-renewal is also fundamental to understanding the regulation of cancer cell proliferation, because cancer can be considered to be a disease of unregulated self-renewal (Reya et al. 2001). Another distinguishing hallmark of stem cells is the ability to undergo asymmetric division, during which stem cells give rise to daughter cells of different fates, proliferative potential, size or other characteristics (Majumdar and Liu 2020; Hitomi et al. 2021a). Cancer stem cells (CSCs) generate such diverse progeny by executing multiple modes of cell division. Lineage-tracing experiments in glioma stem cells (GSCs) revealed that CSC undergo three main types of cell division: 1) Symmetric CSC self-renewing division, where a CSC produces two daughter CSCs; 2) symmetric differentiating division, where a CSC gives rise to two non-CSC daughter cells; 3) asymmetric division, where a CSC produces one CSC and one non-CSC. Additionally less than 1% of cell divisions resulted in cell death (Lathia et al. 2011). The types of CSC cell division are summarized in Figure 2.1.

Numerous arguments suggest a stem-cell origin for human cancers. First, it is worth noting that stem cells possess many of the features that constitute the tumour phenotype, including self-renewal and essentially unlimited replicative potential (Hanahan and Weinberg 2000). Second, the mutations that initiate tumour formation seem to accumulate in cells that persist throughout a person's life, as suggested by the exponential increase of cancer incidence with age (Meza et al. 2008). This is thought to reflect a requirement for between four and seven mutations in a single cell (and its progeny) to effect malignant transformation (Hanahan and Weinberg 2000). Similarly, cancer formation from cells that persist throughout life is suggested by an increased incidence in adults of skin tumours such as melanoma after

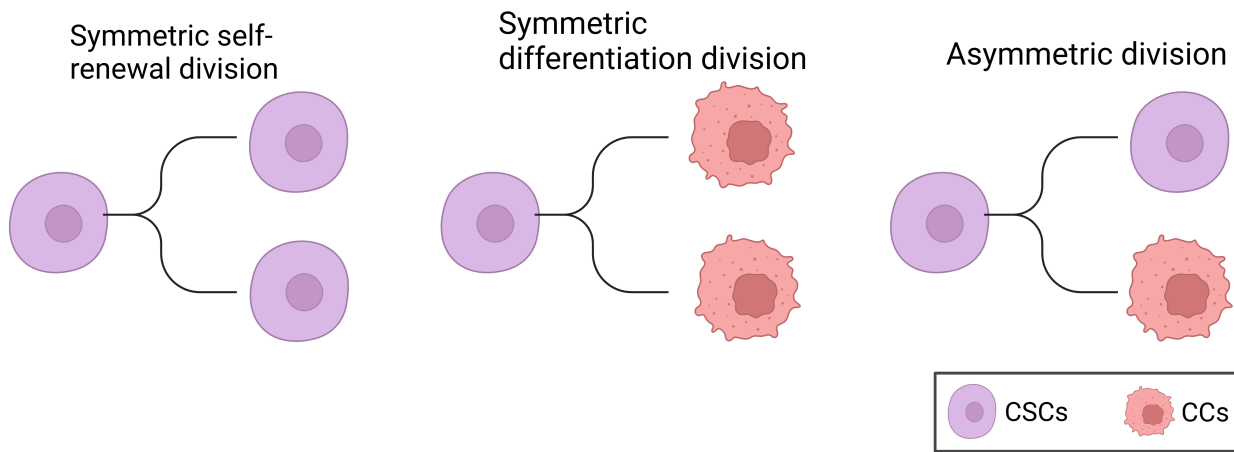


Figure 2.1: The three main types of CSC cell division. Symmetric self-renewal results in two daughter CSCs. Symmetric differentiation results in two non-CSC daughter cells. Asymmetric differentiation results in one CSC and one non-CSC. Non-CSCs are denoted CC for cancer cells (created with BioRender.com).

higher childhood exposure to a mutagenic agent such as ultraviolet solar radiation (Balk 2011). Normal somatic stem cells are strong candidates for such persistent cells, an alternative explanation would be that a more mature cell undergoes a dedifferentiation event, reverting to a more primitive stem cell phenotype (Sell 1993; Reya et al. 2001).

A stem cell origin for human cancers was first identified in leukaemia, perhaps due to the high fraction of stem cells in the haematopoietic system, when it was discovered that some, but not all, cancer cells were able to initiate tumours of the blood (Taipale and Beachy 2001; Lapidot et al. 1994; Bonnet and Dick 1997). More recently CSCs have been identified in many solid tumours including breast, colon and brain (Al-Hajj et al. 2003; Ricci-Vitiani et al. 2007; Ignatova et al. 2002; Hemmati et al. 2003; Singh et al. 2004; Galli et al. 2004). In GBM, cells expressing the CD133 cell surface protein marker (also found on neural stem cells) have been identified as having stem cell properties *in vitro* (Singh et al. 2003). Furthermore, when tested using a xenograft assay, it was found that injection of as few as 100 CD133+ cells produced a tumour that could be serially transplanted and was phenotypically similar to the patient's original tumour, while injection of 10^5 CD133- cells survived in the host but did not cause a tumour (Singh et al. 2004). This provides strong evidence that there is a small subpopulation of glioma stem cells that have the unique ability to initiate tumours, while the majority of cells cannot.

2.3 Cancer stem cells and treatment resistance

Radiation therapy is the most common form of treatment across all cancers, with around 50% of all cancer patients receiving radiotherapy at some point in their treatment (Baskar et al. 2012). However, in addition to being tumour-initiating, CSCs are highly resistant to both radio- and chemo-therapy through preferential activation of the DNA damage checkpoint response and an increase in DNA repair capacity (Bao et al. 2006; Tang et al. 2021a; Rich 2007; Schonberg et al. 2014). In glioma, experimental results

have shown that both in culture and mouse models CD133-expressing stem cells survive radiation in larger proportions than the majority of tumour cells which lack CD133 expression (Bao et al. 2006; Gao et al. 2013); these results suggest that CSC confer radio-resistance in GBM and ultimately are the source of tumour recurrence after radiation.

In addition to being resistant to treatment CSCs also engage in a synergistic relationship with the surrounding tumour microenvironment to promote angiogenesis, proliferation, migration, tumour survival, and immune evasion (Ma et al. 2018; Rich 2007). Taken together this highlights the important role CSCs play in determining tumour response to therapy. There is a desperate need for targeted therapies that either directly kill CSCs or sensitize CSCs to standard cytotoxic therapies in order to improve treatment outcomes.

2.4 Mathematical models of cancer stem cell dynamics

Many different mathematical models have been developed to model stem cell dynamics. Understanding CSC kinetics and interaction with their non-stem counterparts is still limited; theoretical and mathematical models may help elucidate their role in cancer progression and treatment response. Here we focus on a subset of models used in the literature that cover a wide range of modelling techniques and have particularly inspired our modelling used in the preprint presented at the end of this report.

Many of the following models use slightly different terminology to refer to the non-stem cell population such as cancer cell, progenitor cells or tumour cells, for clarity we will refer to non-stem cells always as cancer cells (CCs) throughout this review.

2.4.1 Agent-based models

In (Enderling et al. 2009) and (Gao et al. 2013) the authors develop an agent-based model (ABM) to study the dynamics of CSCs and CCs in a tumour. It is assumed that tumours are a heterogenous mix of CSCs and CCs. Cells are considered as individual entities with a cell cycle and limited proliferation capacity $\rho \in [0, \rho_{\max}]$. CSCs have unlimited self-renewal, hence $\rho_{\max} = \infty$. At each cell division CSCs can undergo symmetric self-renewing division with probability δ or asymmetric division with probability $1 - \delta$. The proliferation capacity ρ is decremented at each CC division and inherited by both daughter cells.

Simulations of the ABM model revealed the following key results:

- Tumours developing solely from CCs will inevitably die out, due to their limited proliferation capacity. Hence, CSCs are necessary for malignant tumour growth. This is consistent with experimental results showing only CSCs can initiate tumours (Lapidot et al. 1994; Singh et al. 2004).
- Tumours started from a single CC could still persist for a long time as long-term dormant lesions, but due to space-limited growth remain small – well below the potential maximum size of $2^{\rho_{\max}}$. Significant growth only occurs once a CSC is initiated. In fact, even with a single CSC, the tumour may remain small for an extended period due to space-limited growth. This is consistent with the observation that many tumours remain dormant for many years before they start to grow (Sweeney 1995; Neves-E-Castro 2006; Folkman and Kalluri 2004).

- A high rate of spontaneous death of CCs actually enables room for sufficient stem cell divisions to enrich the stem cell pool and drive tumour growth. This leads to what they call the “tumour growth paradox”, where counterintuitively an increase in the death rate of CCs decreases the total tumour size in the short term, in the long run it leads to an increase in the total tumour size as the tumour contains more CSCs.

Mathematically the tumour growth paradox is defined as follows.

Definition 2.1 (Tumour growth paradox). Let $N_\alpha(t)$ denote a total tumour population with death rate α for CCs. The population exhibits a tumour growth paradox if there exist death rates $\alpha_1 < \alpha_2$ and times t_1, t_2, T and T_0 such that

$$\begin{aligned} N_{\alpha_1}(t_1) &= N_{\alpha_2}(t_2) \quad \text{and} \quad N_{\alpha_1}(t_1 + T) < N_{\alpha_2}(t_2 + T) \\ &\text{for } (0 < T < T_0), \end{aligned} \tag{2.1}$$

2.4.2 Integro-differential model

Following on from the ABM developed in (Enderling et al. 2009; Gao et al. 2013), in (Hillen, Enderling, and Hahnfeldt 2013) the authors develop an integro-differential equation version of the model, based on the same assumptions as in (Enderling et al. 2009; Gao et al. 2013) outlined in Section 2.4.1. Let $u(x, t)$ denote the density, in cells per unit space, and let $v(x, t)$ denote the density of CCs. Hence, the total tumour density is denoted $N(x, t) = u(x, t) + v(x, t)$. For this analysis cells are assumed to be very small compared to the size of the tissue domain Ω (which we take without loss of generality to have unit volume). It is also assumed that cells cannot pile on top of each other so there is a maximum density of one cell per unit space, this implies $N(x, t) \leq 1$. Cells can only proliferate if there is space to place the daughter cells, otherwise reproduction is inhibited (cellular quiescence). To model the spatial search for space, they define a nonlinear integral term, consistent with the ABM (Enderling et al. 2009; Gao et al. 2013) they assume that all cells can migrate randomly, which is modelled by simple diffusion. These assumptions lead to the following system of equations to describe CSC and CC dynamics:

$$\begin{aligned} \underbrace{\frac{\partial u(x, t)}{\partial t}}_{\text{Rate of change CSCs}} &= \underbrace{D_u \nabla^2 u}_{\text{Diffusion of CSCs}} + \underbrace{\delta \gamma \int_{\Omega} k(x, y, N(x, t)) u(y, t) dy}_{\text{Self-renewal of CSCs}} \\ \underbrace{\frac{\partial v(x, t)}{\partial t}}_{\text{Rate of change CCs}} &= \underbrace{D_v \nabla^2 v}_{\text{Diffusion of CCs}} + \underbrace{(1 - \delta) \gamma \int_{\Omega} k(x, y, N(x, t)) u(y, t) dy}_{\text{Differentiation of CSCs}} + \\ &\quad \underbrace{\rho \int_{\Omega} k(x, y, N(x, t)) v(y, t) dy - \frac{\alpha v}{\alpha v}}_{\text{Proliferation of CCs}} - \underbrace{\frac{\alpha v}{\alpha v}}_{\text{Apoptosis of CCs}}. \end{aligned} \tag{2.2}$$

The spatial distribution kernel $k(x, y, N)$ describes the rate of progeny contribution to location x for a cell at location y per “cell cycle time” i.e., the defined period between divisions of a freely cycling cell. Since greater density at x would be expected to hinder progeny occupation it is assumed that k is monotonically decreasing in N , with $k(x, y, N(x, t)) = 0$ at $N = 1$. The number of cell cycle times per

unit time of CSCs and CCs are denoted by γ and ρ , respectively, and for simplicity it is assumed that $\gamma = \rho = 1$ throughout. The parameter δ with $0 \leq \delta \leq 1$, as in the ABM (Enderling et al. 2009; Gao et al. 2013), denotes the fraction of CSC divisions that are symmetric self-renewal, while $1 - \delta$ is the fraction of asymmetric divisions. The parameter α denotes the spontaneous death rate of CCs. Background cell motility is modelled by the diffusion coefficients D_u and D_v for CSCs and CCs, respectively. The system is considered to hold in a smooth bounded domain Ω , with homogeneous Neumann or Dirichlet boundary conditions.

Homogeneous Neumann boundary conditions correspond to a boundary that is impenetrable by cells, this could for example represent a tissue surrounded by membranes, smooth muscle tissue, or bone, and are given by

$$\frac{\partial u}{\partial n} = 0, \quad \frac{\partial v}{\partial n} = 0 \quad \text{on} \quad \partial\Omega, \quad (2.3)$$

where $\partial/\partial n$ is the normal derivative at the boundary. The redistribution kernel can only redistribute cells within this domain Ω , hence we impose

$$k(x, y, N) = 0 \quad \text{for} \quad x \notin \Omega. \quad (2.4)$$

Homogeneous Dirichlet boundary conditions correspond to a boundary that cells can freely leave but not re-enter again, for example this could represent intravasation into adjacent blood vessels, and are given by

$$u = 0, \quad v = 0 \quad \text{on} \quad \partial\Omega. \quad (2.5)$$

The redistribution kernel describes transport of cells out of the domain but does not allow entering from the outside in, hence

$$k(x, y, N) = 0 \quad \text{for} \quad y \notin \Omega. \quad (2.6)$$

Based on these two boundary conditions we can model any combination of domains such as partially covered by membranes, partially permeable membranes and adjacent blood vessels.

2.4.3 ODE model reduction

In order to analyse this model analytically (Hillen, Enderling, and Hahnfeldt 2013) reduce the system of integro-differential equations (Equation 2.2) to a system of ordinary differential equations in the following way.

Reduction 1: Progeny placement depends only on the density at the destination

In this case $k(x, y, N(x, t)) = k(N(x, t))$. Introducing mean densities which, given that the domain Ω has unit volume, can be written as

$$\bar{u}(t) = \int_{\Omega} u(y, t) dy, \quad \bar{v}(t) = \int_{\Omega} v(y, t) dy, \quad \bar{N}(t) = \bar{u}(t) + \bar{v}(t). \quad (2.7)$$

Then Equation 2.2 becomes:

$$\begin{aligned} u_t(x, t) &= D_u \nabla^2 u(x, t) + \delta k(N(x, t)) \bar{u}(t), \\ v_t(x, t) &= D_v \nabla^2 v(x, t) + (1 - \delta) k(N(x, t)) \bar{u}(t) + k(N(x, t)) \bar{v}(t) - \alpha v(x, t). \end{aligned} \quad (2.8)$$

Reduction 2: Density is uniform across the domain

If tumour growth is assumed uniform across the domain then, $k(N(x, t)) = k(\bar{N}(t))$ and $u(x, t)$ and $v(x, t)$ can be replaced with their spatially averaged values ($\bar{u}(t)$ and $\bar{v}(t)$) and diffusion is zero everywhere. Therefore, Equation 2.8 becomes:

$$\begin{aligned} \frac{d\bar{u}}{dt} &= \delta k(\bar{N}(t)) \bar{u}, \\ \frac{d\bar{v}}{dt} &= (1 - \delta) k(\bar{N}(t)) \bar{u} + k(\bar{N}(t)) \bar{v} - \alpha \bar{v}(t), \end{aligned} \quad (2.9)$$

where the volume filling constraint $k(\bar{N})$ is taken to be

$$k(\bar{N}) = \max \{0, 1 - \bar{N}^\sigma\}, \quad \text{for } \sigma > 1. \quad (2.10)$$

An exponent of $\sigma = 1$ corresponds to a linearly decreasing rate of occupancy for newborn cells as the total density \bar{N} increases. Since cells are nonrigid, deformable and able to squeeze into available spaces (Hillen, Enderling, and Hahnfeldt 2013) argue that $\sigma > 1$ is appropriate and take it to be $\sigma = 4$, in all their simulations.

Without a CSC population $\bar{u}(t)$, the density of CCs $\bar{v}(t)$ satisfies the equation

$$\frac{d\bar{v}}{dt} = K(\bar{v}(t)) \bar{v}(t) - \alpha \bar{v}(t). \quad (2.11)$$

Since $K(\bar{v}(t))$ is a decreasing function of $\bar{v}(t)$ the CC population will die out when $\alpha > k(0)$. Note that this does not specifically set a limited proliferation capacity for CCs, as was the case in (Enderling et al. 2009), rather if $\alpha > k(0)$ then $\alpha > k(N)$ for all N hence the CC population will never survive on its own.

This simpler ODE model allows for analysis of the steady states, from which it can be shown that the pure stem cell steady state $(u, v) = (1, 0)$ is a global attractor. Therefore, this model predicts that for long times the tumour will consist of only stem cells. Intermediate tumour composition and the time at which the steady state is achieved are dependent on cell death rate α . The convergence to $(1, 0)$ is somewhat surprising as typically the CSC compartment is considered small, comprising only 1-3% of the total tumour (Bao et al. 2006). This suggests that the model may miss key biological dynamics of the CSCs such as some stem cell death and feedback regulation of symmetric / asymmetric division. However, (Hillen, Enderling, and Hahnfeldt 2013) argue that this does not interfere with their analysis, as they are

interested in the intermediate time dynamics of tumour initiation and growth, rather than the long-term behaviour as $t \rightarrow \infty$.

2.4.4 Stochastic model of CSC dynamics

In (Turner et al. 2009), the authors develop a stochastic model for the dynamics of CSCs and CCs, particularly for the case of brain cancer. This stochastic model is particularly appropriate for situations in which small numbers of cells are present such as *in vitro* or in the early stages of tumour formation. In these cases stochastic fluctuations may have significant effects and cannot be neglected. To study larger populations the authors then derive a deterministic ODE model, based on the stochastic master equation, that describes the average number of CSCs and CCs.

The model assumptions on CSCs and CCs are largely similar as those given previously in Section 2.4.1. However, one key difference is that CSCs are assumed not to be immortal so have some probability of death. Defining $p(n_s, n_p, t)$ as the probability that there are exactly n_s CSCs and n_p CCs at time t , the stochastic master equation is given by

$$\frac{dp(n_s, n_p, t)}{dt} = \rho_s \left[\underbrace{r_1(n_s - 1)p(n_s - 1, n_p, t)}_{\text{symmetric self renewal of CSCs}} \right. \\ + \underbrace{r_2 n_s p(n_s, n_p - 1, t)}_{\text{asymmetric division of CSCs}} \\ + \underbrace{r_3(n_s + 1)p(n_s + 1, n_p - 2, t)}_{\text{symmetric differentiation of CSCs}} \\ \left. - \underbrace{n_s p(n_s, n_p, t)}_{\text{Overall division}} \right] \\ + \underbrace{\Gamma_s [(n_s + 1)p(n_s + 1, n_p, t) - n_s p(n_s, n_p, t)]}_{\text{Apoptosis of CSCs}} \\ + \underbrace{\Gamma_p [(n_p + 1)p(n_s, n_p + 1, t) - n_p p(n_s, n_p, t)]}_{\text{Apoptosis of CCs}}. \quad (2.12)$$

This model explicitly accounts for all three types of CSC division shown in Figure 2.1 where r_1 = symmetric self renewal probability, r_2 = asymmetric division probability, r_3 = symmetric differentiation probability, and ρ_s represents the overall CSC division rate. While the model in Section 2.4.2 only accounts for asymmetric division it can be shown that these two formulations are equivalent for a large set of parameter values (Hillen, Enderling, and Hahnfeldt 2013). The parameters Γ_s and Γ_p represent the rate of apoptosis for CSCs and CCs respectively. Due to the model's stochastic nature, and the inclusion of a death probability for CSCs, it can be shown that the occurrence of a single CSC will not necessarily result in a tumour, even if the probability of self-renewal is greater than the probability of differentiation. This is in contrast to the previous models discussed (Enderling et al. 2009; Hillen, Enderling, and Hahnfeldt 2013) and to a deterministic version of this model (Equation 2.13) that would predict exponential growth of the tumour from a single CSC.

For larger cellular populations it becomes more challenging to simulate such a stochastic model and it becomes pertinent to consider the equations for the average number of CSCs and CCs. Defining the mean cellular populations $S = \langle n_s \rangle$, $P = \langle n_p \rangle$ and $r = r_1 - r_3$ (i.e., the difference in symmetric self-renewal division and asymmetric differentiation division), the deterministic model is given by

$$\begin{aligned}\frac{dS}{dt} &= \rho_s r S - \Gamma_s S, \\ \frac{dP}{dt} &= \rho_s (1 - r) S - \Gamma_p P.\end{aligned}\tag{2.13}$$

This model is largely similar to the ODE model presented in (Hillen, Enderling, and Hahnfeldt 2013), Equation 2.9. The main differences are that Equation 2.13 includes a rate of CSC apoptosis Γ_s and Equation 2.13 does not account for completion for space. Although (Turner et al. 2009) introduce this into a later version of the model, where they take ρ_s to be given by $\rho_s(S, P) = \rho_s(1 - c_s S - c_p P)$, where $1/c_s$ and $1/c_p$ are the limiting populations of stem and CCs respectively. However, a limitation of this approach is that it does not account for competition between CSCs and CCs for space and resources.

2.4.5 A multispecies PDE model of cell lineages

In (Youssefpour et al. 2012) the authors develop a multispecies PDE model for CSC lineage dynamics. This is the first model we have looked at that considers more than the two cell types, CSCs and CCs. Here the model is more complex and accounts for CSCs, committed progenitor cells, terminal cells, and dead cells. As with the previous models we have looked at it is assumed that differentiation and feedback processes link the cells' lineage through self-renewal fractions and mitosis rates. The dependent variables in the model are the local volume fractions of the cell species denoted $\phi_{\text{CSC}}, \phi_{\text{CP}}, \phi_{\text{TC}}, \phi_{\text{DC}}$, as well as healthy cells and water $\phi_{\text{H}}, \phi_{\text{W}}$. Assuming there are no voids the sum of the volume fractions equals 1 and each cell type follows a conservation equation of the form

$$\frac{\partial \phi}{\partial t} = -\nabla \cdot J - \nabla \cdot (u_s \phi) + S\tag{2.14}$$

where ϕ denotes the volume fraction of the cell type, J is generalized diffusion, u_s is the mass-averaged velocity of the solid components, S denotes the mass-exchange terms. This type of multiphase volume fraction approach has been widely used in cancer modelling (Lowengrub et al. 2010; Breward 2003; Hubbard and Byrne 2013). Simulation of this model show that the distributions of cell populations obtained from ABM model (Enderling et al. 2009) and this multispecies model are different. In the ABM CSCs tend to be located either at the center of small tumour clusters or distributed relatively uniformly throughout the tumour, some CSCs may migrate past the tumour boundary and generate new tumour clusters that eventually join the primary cluster creating an irregular boundary. On the other hand, the continuum model finds that CSCs tend to be located at the boundary of sufficient large tumour spheroids, this is consistent with some experiments (Vlashi et al. 2009). For smaller spheroids the CSCs may be more uniformly distributed. The patterns of CSCs and CCs are due to the cell signalling model implemented, detailed in Section 2.5.1, where the CSC self-renewal fraction is regulated by feedback factors produced by the different cell types (Youssefpour et al. 2012).

2.5 Models of differentiation therapy

If, as with normal tissues, cellular phenotypic heterogeneity within tumours can be explained by a hierarchy of differentiation, with only a subset of stem-like cells capable of long-term self-renewal, this raises the prospect that signals promoting differentiation could be effective at driving malignant cells to a less aggressive and ideally post-mitotic differentiated state (Carén, Beck, and Pollard 2016). This differentiation therapy approach has seen success in acute promyelocytic leukemia (APL) where all-trans-retinoic acid (ATRA) can promote differentiation of CSCs and lead to complete remission (Yan and Liu 2016; De Thé 2018). In GBM, bone morphogenetic protein 4 (BMP4), a member of the TGF- β superfamily, has shown potential as a differentiation therapeutic agent. BMP4 has been shown to drive differentiation of GSCs towards a predominantly glial (astrocytic) fate, to reduce GBM tumour burden *in vivo* and to improve survival in a mouse model of GBM (Nayak et al. 2020; Piccirillo et al. 2006). Despite its potential as a treatment option relatively few mathematical models have considered its possible effects on tumour growth (Youssefpour et al. 2012; Bachman and Hillen 2013; Turner et al. 2009).

2.5.1 Differentiation promoter and self-renewal promoter

In (Youssefpour et al. 2012) they follow (Lander et al. 2009) and assume that the proliferation and differentiation of CSCs are regulated by factors in the tumour microenvironment that feedback on self-renewal fractions and mitosis rates. In particular, they denote the differentiation promoter T (for TGF- β superfamily members) that reduces the probability of self-renewal for CSCs. They also account for self-renewal promoter W which increases the probability of self-renewal of CSCs, as well as an inhibitor of W denoted WI . Possible self-renewal promoters include WNTs, Notch and Shh (Pannuti et al. 2010; Bailey, Singh, and Hollingsworth 2007). Using the notation introduced in Section 2.4.5, they define the CSC self-renewal fraction as

$$P_s = P_{\min} + (P_{\max} - P_{\min}) \left(\frac{\xi C_w}{1 + \xi C_W} \right) \left(\frac{1}{1 + \psi C_T} \right), \quad (2.15)$$

where P_{\min} and P_{\max} are the minimum and maximum probability of CSC self-renewal, taken to be 0.2 and 1 respectively. C_W and C_T represent the concentrations of the self-renewal promoter and differentiation promoter respectively. The parameters ξ and ψ quantify the sensitivity of CSCs to the regulating proteins.

The concentrations of differentiation promoter and self-renewal promoter are then modelled as follows. It is assumed that T is more diffuse than either W or WI . Therefore, on the time scale of cellular proliferation they make the quasi-steady-state assumption that time derivatives and advection of T can be neglected. Thus, the quasi-steady reaction-diffusion equation for C_T is given by

$$0 = \nabla \cdot (D_T \nabla C_T) - (\nu_{UT} \phi + \nu_{DT}) C_T + \nu_{PT} \phi_{TC} \quad (2.16)$$

where D_T is the diffusion coefficient, ν_{UT} , ν_{DT} and ν_{PT} are the uptake rate by CSCs, the rate of decay and the rate of production by the terminal cells, respectively.

To model the self-renewal promoter W and its inhibitor WI a generalized Gierer-Meinhard-Turing system of reaction advection diffusion equations is used, given by

$$\begin{aligned}\frac{\partial C_W}{\partial t} + \nabla \cdot (u_s C_W) &= \nabla \cdot (D_W \nabla C_W) + f(C_W, C_{WI}), \\ \frac{\partial C_{WI}}{\partial t} + \nabla \cdot (u_s C_{WI}) &= \nabla \cdot (D_{WI} \nabla C_{WI}) + g(C_W, C_{WI}),\end{aligned}\tag{2.17}$$

where

$$\begin{aligned}f(C_W, C_{WI}) &= \nu_{PW} \frac{C_W^2}{C_{WI}} C_0 \phi_{CSC} - \nu_{DW} C_W + u_0 C_0 (\phi_{CSC} + \phi_{CP} + \phi_{TC}), \\ g(C_W, C_{WI}) &= \nu_{PWI} C_W^2 C_0 \phi_{CSC} - \nu_{DWI} C_{WI}.\end{aligned}\tag{2.18}$$

The parameters D_W and D_{WI} are the diffusion coefficients, ν_{PW} , ν_{DW} and ν_{PWI} , ν_{DWI} are the production and decay rates of W and WI respectively. The parameter u_0 represents a low-level source of W from all the tumour cells.

To model differentiation therapy (Youssefpour et al. 2012) fix $\psi = 0.5$ and introduce an external source of T i.e., a constant source term is added to Equation 2.16.

2.5.2 No self-renewal promoter

In (Bachman and Hillen 2013) they follow (Youssefpour et al. 2012) and model differentiation therapy through a relationship between the average level of differentiation promoter, which they denote C_F and the probability of CSC self-renewal P_s . However, they do not include the effects of a CSC self-renewal promoting factor, thus

$$P_s(t) = P_{\min} + (P_{\max} - P_{\min}) \left(\frac{1}{1 + \psi C_F(t)} \right),\tag{2.19}$$

where the notation is the same as in Equation 2.15. Since (Bachman and Hillen 2013) do not model endogenous production of differentiation promoter, C_F solely represents the level of differentiation promoter prescribed during differentiation therapy. To address this lack of endogenous differentiation promoters they take $P_{\max} = 0.505$ (which is equivalent to setting $\delta = 0.01$ as was done in (Hillen, Enderling, and Hahnfeldt 2013)) and $P_{\min} = 0.2$, as is done in (Youssefpour et al. 2012).

As (Bachman and Hillen 2013) use the ODE model developed in (Hillen, Enderling, and Hahnfeldt 2013) they must also develop a submodel for the average level of differentiation promoter. As it is an ODE model they consider the average level of differentiation promoter within a spatially homogeneous tumour $C_F(t)$. It is assumed that the tumour resides within a spherical region of tissue and that differentiation promoter enters this area through the boundary. The differentiation promoter enters the region from the boundary and will diffuse very quickly and attain a steady state distribution over this region. To compute the value of $C_F(t)$ they solve the problem of diffusion over a sphere of radius R and average the solution over the volume of the sphere. We use the lower case letter to describe the radial symmetric solution $c_F(r, t)$ of the following boundary value problem

$$\frac{\partial c_F}{\partial t} = \omega \left(\frac{\partial}{\partial r} \left(\frac{\partial c_F}{\partial r} \right) + \frac{2}{r} \frac{\partial c_f}{\partial r} \right) \quad (2.20)$$

$$c_F(R, t) = C_{F0}(t),$$

where ω is the effective diffusivity of the differentiation promoter. Before differentiation therapy begins $C_{F0}(t) = 0$, when differentiation therapy begins the boundary condition on the sphere is set to $C_{F0}(t) = 1$, and the promoter diffuses into the sphere. When differentiation therapy ends, the boundary condition is simply set to 0 and the promoter diffuses out of the sphere. They then set

$$C_F(t) = \frac{3}{R^3} = \int_0^R c_F(r, t) r^2 dr. \quad (2.21)$$

2.5.3 BMP4 in glioma

In the previous models (Youssefpour et al. 2012; Hillen, Enderling, and Hahnfeldt 2013) they considered a general differentiation promoter, in (Turner et al. 2009) they consider the specific differentiation promoter BMP4 in GBM. As in the case for the general differentiation promoter they interpret the effects of BMP4 as decreasing the net symmetric division rate r (following the notation used in Section 2.4.4). Based on (Piccirillo et al. 2006) they estimate that from a pre-treatment value of $r = 0.1$ the effect of BMP4 is to reduce r to -0.1 , note that following the notation used in Section 2.4.4 r is defined as $r = r_1 - r_3$ so a change of r to negative represents a both an increase in the proportion of symmetric differentiation divisions and a decrease in symmetric self-renewal divisions. To model differentiation therapy the parameter value r is simply switched between these two values for the duration of BMP4 exposure.

2.5.4 Summary of differentiation therapy results

All the models compare 3 different treatment cases radiation alone, differentiation therapy alone and combination therapy. Importantly, as has been shown, all models assume that CSCs are less sensitive to radiation than CCs (Bao et al. 2006; Tang et al. 2021b; Hitomi et al. 2021b). Despite the slight differences in assumptions and implementation, all models find similar results. Radiotherapy alone fails as some CSCs survive and are able to repopulate the tumour. In fact, all models show an extension of the “tumour growth paradox” which we term the “tumour treatment paradox”. When treating with radiation alone the fraction of CSCs increases, since the CCs are more susceptible they significantly reduce their numbers leaving more room for CSCs. This CSC enriched post-treatment state allows much more rapid re-growth of the tumour. This suggests that current standard of care treatment selects for the more resistant CSCs. Thus treatment often facilitates more rapid and aggressive tumour recurrence. Differentiation therapy alone can successfully eradicate the tumour, however, given all models assume that CSCs can only transform into CCs through cellular division, rather than direct transition, large intermediate values of total tumour size may be reached using this approach. Combination of differentiation and radiotherapy out performed either single therapies, often showing that the tumour can be driven to much smaller sizes and potentially extinction. This is because the differentiation agent induces CSCs to turn into CCs which then can be killed by traditional radiation therapy. This combination therapy can be considered a new class of strategies for cancer therapy known as evolutionary steering approaches. Rather than reactively

altering treatment as resistance is acquired we proactively select our treatment to minimise resistance and increase chance of extinction ([Enriquez-Navas, Wojtkowiak, and Gatenby 2015](#); [Acar et al. 2020](#)).

2.6 Conclusion

In summary, mathematical models of CSC dynamics provide valuable insights into tumour growth, dormancy, and response to treatment. While the models reviewed here vary in their complexity and underlying assumptions, they all highlight the critical role of CSCs in tumour maintenance, treatment resistance and tumour recurrence. Mathematical modelling provides a unique tool for analysing the non-trivial interaction between CSCs and CCs that can arise from fairly simple assumptions, allowing us to verify or generate new hypothesis in order to better understand the role of CSCs.

The differentiation therapy approach aims to drive CSCs within tumours toward a differentiated state, potentially mitigating their self-renewal capacity and aggressiveness. Despite this, many challenges remain in developing differentiation therapies that can be used in a clinical setting ([Carén, Beck, and Pollard 2016](#)). One key challenge particularly in GBM is delivery of differentiation therapy to the tumour microenvironment, due to the blood brain barrier (BBB) which limits transport into the brain. New delivery mechanism to combat this are being developed such as adipose derived mesenchymal stem cells, containing BMP4 in nanoparticles. These can be delivered directly into the tumour at the time of resection or systemically as they have been shown to cross the BBB ([Li et al. 2014a](#); [Mangraviti et al. 2016a](#); [Pendleton et al. 2013a](#)). Additionally as with all therapies there is vast heterogeneity between patient response to differentiation therapy, indicating the importance of identifying biomarkers for sensitivity to such therapies. In work in preparation it has been shown that GBM cell lines that did not express pRBS were unresponsive to differentiation therapy ([Farias et al., n.d.a](#)). Mathematical modelling may also help improve the effectiveness of differentiation therapy strategies optimising its delivery in combination with standard cytotoxic therapies as well as elucidating the mechanism through which CSCs drive tumour growth.

In the next chapter I present our preprint, looking at a model for BMP4 induced differentiation therapy in GBM, which is available on bioRxiv [Virtual Clinical Trials of BMP4 Differentiation Therapy: Digital Twins to Aid Glioblastoma Trial Design](#).

3 Virtual Clinical Trials of BMP4 Differentiation Therapy: Digital Twins to Aid Glioblastoma Trial Design

We leverage an integrative mathematical modeling framework to translate the impact of preclinical findings in virtual clinical trials. We develop a virtual clinical trial pipeline to face the real-world problem of numerous of actual early phase clinical trials that have failed for glioma/glioblastoma, the most common primary brain tumor. Even with the most promising preclinical data, designing clinical trials is fraught with challenges, including controlling for the many parameters used to inform patient selection criteria. Here, we introduce a virtual trial pipeline that allows us to consider the variability from some of these criteria that can be used for future trials of novel therapies. As an example, we apply this to the proposed delivery of BMP4 to stem cell niches present in glioblastoma, the most aggressive glioma, known for its inter- and intra-patient heterogeneity. The proposed approach of BMP4 treatment, delivered through adipose-derived mesenchymal stem cells, aims to promote cellular differentiation away from the treatment-resistance stem cell niches towards a more treatment-vulnerable state. This pipeline will help us narrow down strategies for future trials, optimize timing of treatments relative to key standard-of-care treatments, and predict synergy amongst the developed treatments.

3.1 Introduction

Glioblastoma (GBM) is the most commonly diagnosed primary malignant brain cancer in adults. Current standard of care consists of maximal safe surgical resection followed by concurrent radiotherapy and chemotherapy (with temozolomide) (Stupp et al. 2005). Despite this aggressive treatment, outcomes remain poor with median survival of only 15 months (Ostrom et al. 2019). The aggressiveness and fatal outcomes of GBM can be attributed to its highly infiltrative nature and to its vast intra- and inter-patient heterogeneity. Malignant cells can be found infiltrating far into the peritumoral areas of the brain and are undetectable by conventional imaging and operative techniques. Furthermore, tumors contain an array of different cell types with distinct molecular and phenotypic characteristics, hindering therapy efficacy. In particular, previous studies have identified a sub-population of malignant glioma cells with stem-like characteristics known as glioma stem cells (GSCs) or brain tumor initiating cells (BTICs). These cells are highly resistant to both radio- and chemo-therapy and therefore contribute to treatment failure (Bao et al. 2006; Singh et al. 2004). Thus, if treatment outcomes are to be improved for patients with GBM, it is vital that therapeutics that specifically target these GSCs are developed.

The existence of a population of cancer stem cells (CSCs) was first established in leukemia (Lapidot et al. 1994; Bonnet and Dick 1997). More recently CSCs have been identified in many solid tumors including breast, colon and brain (Al-Hajj et al. 2003; Ricci-Vitiani et al. 2007; Ignatova et al. 2002; Hemmati et al. 2003; Singh et al. 2004; Galli et al. 2004). In GBM, cells expressing the CD133 cell surface protein marker (also found on neural stem cells) have been identified as GSCs based on their exclusive ability to commence and support tumor growth (Singh et al. 2004). In addition to being tumor initiating, GSCs are highly resistant to both radio- and chemo-therapy as they are more efficient at inducing repair of damaged DNA (Bao et al. 2006; Tang et al. 2021a; Rich 2007; Stiles and Rowitch 2008; Schonberg et al. 2014; Turner et al. 2009; Dirks 2006). Furthermore, they also engage in a synergistic relationship with the surrounding tumor microenvironment (TME) to promote angiogenesis, proliferation, migration, tumor survival, and immune evasion (Ma et al. 2018). Under the brain cancer stem cell hypothesis, it is becoming increasingly clear that while radiation may be transiently effective, treatment ultimately fails in the long run if any GSCs survive (Dingli and Michor 2006).

If, as with normal tissues, cellular phenotypic heterogeneity within tumors can be explained by a hierarchy of differentiation, with only a subset of stem-like cells capable of long-term self-renewal (Carén, Beck, and Pollard 2016), this raises the prospect that signals promoting differentiation could be effective at driving malignant cells to a less aggressive and ideally post-mitotic differentiated state. This differentiation therapy approach has seen success in acute promyelocytic leukemia (APL) where all-trans-retinoic acid (ATRA) can promote differentiation of CSCs and lead to complete remission (De Thé 2018; Yan and Liu 2016). In GBM, bone morphogenetic protein 4 (BMP4), a member of the TGF- β superfamily, has shown potential as a differentiation therapeutic agent. BMP4 has been shown to drive differentiation of GSCs towards a predominantly glial (astrocytic) fate, to reduce GBM tumor burden *in vivo* and to improve survival in a mouse model of GBM (Nayak et al. 2020; Carén, Beck, and Pollard 2016; Piccirillo et al. 2006). The precise mechanism through which BMP4 acts is unknown but a possible explanation is that it reduces the frequency of symmetric divisions of GSCs (Guerrero-Cázares et al. 2014), and previous mathematical models of differentiation therapy have assumed that differentiation promoters act in this way (Youssefpour et al. 2012; Bachman and Hillen 2013).

Adipose derived mesenchymal stem cells (AMSCs) provide a possible alternative to traditional treatment, as these cells preferentially migrate toward areas of malignancy, and can be utilized to home towards the infiltrating glioma cells (Li et al. 2014b; Mangraviti et al. 2016b; Pendleton et al. 2013b; Smith et al. 2015; Doucette et al. 2011). Additionally AMSCs can be engineered to secrete BMP4 for GBM therapy, and a migration assay showed that compared to controls, engineered AMSCs significantly retained their tropism and preferential migration towards GBM factors (Mangraviti et al. 2016b; J. Kim et al. 2020; Guerrero-Cázares et al. 2014; Tzeng et al. 2011). It has been shown that nanoparticle-engineered AMSCs maintain their multi-potency characteristics and release their therapeutic cargo progressively, furthermore systemically-delivered engineered AMSCs can cross the blood-brain barrier and retain their preferential tropism towards gliomas (Mangraviti et al. 2016b). Therefore, AMSCs delivery promises the ability to hone in on GSC niches and locally release treatment to these regions. BMP4-loaded AMSCS (BMP4-AMSCs) would theoretically migrate to GSCs, release BMP4, and increase the rate of their differentiation, reducing the number of GSCs and increasing sensitivity to standard treatments.

Clinical trials typically consist of four phases in which a new intervention is investigated in human subjects to determine its safety and efficacy. This system is notoriously resource intensive and inefficient. The average cost per patient is \$59,500 and takes more than 10 years, with only 10% of drugs in phase 1 studies eventually approved (Dowden and Munro 2019; Yankeelov et al. 2024). In GBM, the statistics are even

worse; multiple recent phase 3 trials have failed to meet their prespecified primary endpoints (Bagley et al. 2022; Reardon et al. 2020; Cloughesy et al. 2020; Weller et al. 2017; Narita et al. 2019; Roth et al. 2021). Of course, there are many reasons for these failures including inter- and intra-patient variability, drug delivery limitations, paucity of control arms, overly stringent clinical eligibility, and beyond (Bagley et al. 2022).

Increasingly, it is being realised that mathematical modelling and *in silico* clinical trials can assist in addressing a number of these problems. Subfields such as virtual clinical trials (Craig et al. 2023), phase *i* trials (E. Kim et al. 2016), and digital twins (Wu et al. 2022) have evolved all with the aim to create simulated patients or patient cohorts that can be used as a surrogate to predict the effects of treatment on a more personalized level. This approach has been applied to a variety of cancers, including breast cancer (Wang et al. 2019; Wang et al. 2020), head and neck cancer (Zahid et al. 2021), melanoma (E. Kim et al. 2016), and ovarian cancer (Cardinal et al. 2022). Here, we take a similar *in silico* approach to glioblastoma and its proposed treatment with BMP4-AMSCs.

3.2 Materials and methods

We use mathematical modelling to simulate GSC-driven brain tumor growth. Our model describes the interplay of GSCs ($s(t)$) and non-GSCs ($v(t)$). To describe radiation therapy we use the well-established linear quadratic model (R. Rockne et al. 2009; McMahon 2018) with realistic standard treatments (five treatments per week, weekends off, for six weeks) and with tissue-specific radiosensitivity parameters. Following (Bachman and Hillen 2013; Youssefpour et al. 2012) we model differentiation therapy as decreasing the propensity for self-renewal of GSCs.

3.2.1 Pre-clinical data

To quantify the effect of BMP4 on sensitising GSCs, we used data collected from a clonogenic radiotherapy (RT) assay (Farias et al., n.d.b). Five GSC cell lines were treated with either complete media (untreated control), BMP4 (100 ng/ml), BMP4-AMSCs conditioned media (100 ng/ml BMP4), or a similar volume of non-engineered AMSC conditioned media for a period of 48 hours, then seeded at 250-1250 cells per well in 96 well plates and treated with 0, 2, 4, 6 Gy of radiation, with six replicates in each case. After 14 days the colonies with more than 100 nm diameter were manually counted.

Typically, the linear quadratic (LQ) model is used to describe the surviving fraction of cells after radiation. However, this assumes only one cell type is present (R. Rockne et al. 2009; McMahon 2018; Yu et al. 2015). In the control case, GSC lines are cultured in stem cell media, so we assume that cells will remain as GSCs unless any BMP4 or other differentiation promoter is present, thus the LQ model is applicable. However, when BMP4 is applied some amount of differentiation of GSCs will take place that explains the increased sensitivity to RT. To get an estimate for the amount of differentiation that took place over 48hr exposure, we fit a dual-linear quadratic (DLQ) model similar to that of (Yu et al. 2015), given by:

$$\gamma(d) = F \exp(\eta(-\alpha d - \beta d^2)) + (1 - F) \exp(-\alpha d - \beta d^2) \quad (3.1)$$

where d is the RT dose, F is the fraction of GSCs and η is the protection factor for GSCs that accounts for the fact that GSCs are less sensitive to radiation than other cancer cells; previous experiments have estimated GSC radio-protection to be $\eta = 0.1376$ (Gao et al. 2013). We infer the radiobiological parameter from the cell line data in the following way. First, we assume that since the GSC lines are cultured in stem cell media no differentiation will take place, therefore we fit the LQ model to the control case for each cell line, assuming the ratio $\alpha/\beta = 10$ (R. Rockne et al. 2010), to get an estimate for α . These form the cell-line-specific radiosensitivity parameters. Using these parameters we fit the DLQ model to the BMP4 treated survival data, treating α and β as fixed constants for each cell line from the control case so that we are only fitting for F . This allows us to get an estimate of the fraction of GSCs after 48hrs exposure to BMP4 in each cell line. The fitted α and F for all the cell lines are shown in Table 3.1.

3.2.2 Model assumptions and equations

- GSCs have unlimited replicative potential.
- GSCs are capable of both self-renewing and differentiating. Using the same notation as (Youssef-pour et al. 2012) we denote the proportion of GSCs that self-renew by P_s . This does not distinguish between symmetric and asymmetric division, but rather just considers the overall fraction of proliferating cells that self-renew (P_s) and differentiate ($1 - P_s$).
- Progenitor cells (PCs) have a limited replicative potential, this ensures that they are not tumor-initiating. Following (Enderling et al. 2009; Gao et al. 2013), the proliferative potential of PCs is set to a maximum of $n = 10$ divisions. Once PCs have divided $n = 10$ times they become terminally differentiated (TC) and can no longer proliferate.

Figure 3.1 shows a schematic of this model. Following these assumptions, we derive the following equations,

$$\begin{aligned}
 \underbrace{\frac{ds}{dt}}_{\text{Rate of change GSCs}} &= \underbrace{(2P_s - 1)m_s s \left(1 - \frac{N}{k}\right)}_{\text{Self-renewal of GSCs}} - \underbrace{\delta_s s}_{\text{Apoptosis}} , \\
 \underbrace{\frac{dv_1}{dt}}_{\text{Rate of change PCs}} &= \underbrace{2(1 - P_s)m_s s \left(1 - \frac{N}{k}\right)}_{\text{Differentiation of GSCs}} - \underbrace{m_1 v_1 \left(1 - \frac{N}{k}\right)}_{\text{Proliferation of PCs}} - \underbrace{\delta_1 v_1}_{\text{Apoptosis}} , \\
 \underbrace{\frac{dv_i}{dt}}_{\text{Rate of change PCs}} &= \underbrace{2m_{i-1} v_{i-1} \left(1 - \frac{N}{k}\right)}_{\text{Proliferation of PCs}} - \underbrace{m_i v_i \left(1 - \frac{N}{k}\right)}_{\text{Proliferation of PCs}} - \underbrace{\delta_i v_i}_{\text{Apoptosis}} , \quad i = 2, \dots, n-1 \\
 \underbrace{\frac{dv_n}{dt}}_{\text{Rate of change PCs}} &= \underbrace{2m_{n-1} v_{n-1} \left(1 - \frac{N}{k}\right)}_{\text{Differentiation of PCs}} - \underbrace{\delta_n v_n}_{\text{Apoptosis}} ,
 \end{aligned} \tag{3.2}$$

where $s(t)$ is the density of GSCs, $v_i(t)$ is the density of PCs (at proliferation level i) and $v_n(t)$ are terminally differentiated cells. The total density of the tumor is given by $N(t) = s + \sum_{i=1}^n v_i$. The apoptosis rate for GSCs is δ_s and for PCs are given by δ_i . The proliferation rates of GSCs and PCs are

given by m_s , m_i respectively, where we assume all m_i are equal. These proliferation rates are subject to a crowding response, represented by the term $1 - N/k$ where k is the carrying capacity of the tumor.

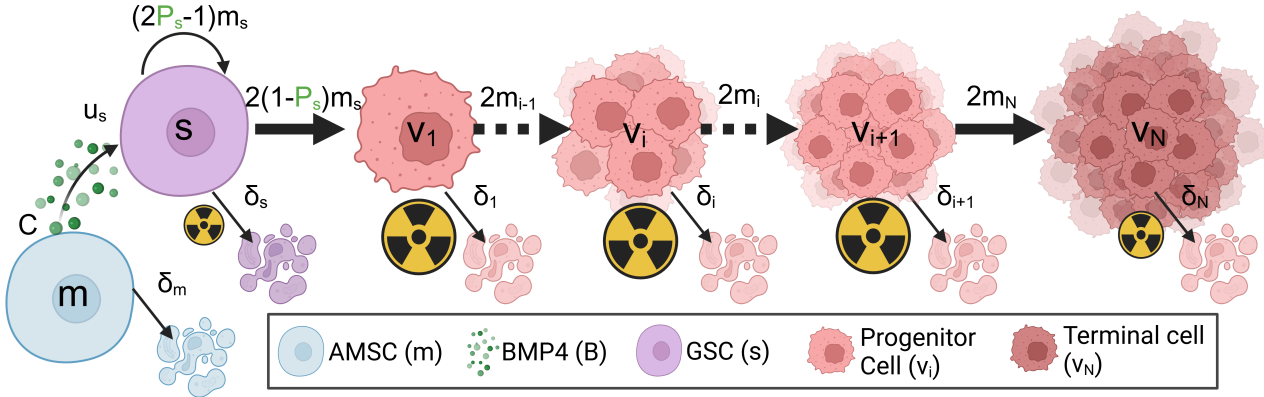


Figure 3.1: Model schematic, showing how GSCs differentiate into progenitor cancer cells which can then divide a number of times, doubling in number each time (Equation 3.2). Eventually, PCs become terminally differentiated and are no longer able to proliferate. Introduced AMSCs gradually die and release BMP4 (Equation 3.3) which modifies the self-renewal rate P_s according to Equation 3.4. (created with BioRender.com)

3.2.2.1 Differentiation therapy with mesenchymal stem cell delivery model

A possible delivery mechanism for BMP4 is via AMSCs. These could be implanted at the time of resection, or systemically with the ability to cross the blood-brain barrier and subsequently diffuse with preferential tropism towards glioma cells. We model AMSCs as simply decaying exponentially from an initial concentration at implantation. BMP4 is released from these AMSCs and taken up by GSCs. The equations for both the AMSC and BMP4 are thus given by.

$$\begin{aligned}
 \frac{dm}{dt} &= \underbrace{-\delta_m m}_{\substack{\text{Rate of} \\ \text{change AMSCs}}} & (3.3) \\
 \frac{dB}{dt} &= \underbrace{Cm}_{\substack{\text{Rate of} \\ \text{change BMP4}}} - \underbrace{u_s B s}_{\substack{\text{Release of BMP4} \\ \text{uptake by GSCs}}} - \underbrace{\delta_B B}_{\text{Decay of BMP4}}
 \end{aligned}$$

where δ_m is the decay rate of AMSCs, C is the rate at which AMSCs release BMP4, u_s is the uptake rate of BMP4 by GSCs and δ_B is the decay rate of BMP4. *In vivo* experiments have shown that AMSCs can survive for around 14 days in a rodent model and that BMP4 reaches its peak concentration at around 48hrs after initial implantation of AMSC (Li et al. 2014b).

3.2.2.2 BMP4 model

Following (Bachman and Hillen 2013), we model differentiation therapy through a simple relationship between the level of differentiation promoter (BMP4), and the probability of GSC self-renewal, P_s , and do not consider the effect of a GSC promoter such as WNT (Lee et al. 2016; Youssefpour et al. 2012). Therefore, the relationship between P_s and BMP4 is given by

$$P_s(t) = P_{\min} + (P_{\max} - P_{\min}) \left(\frac{1}{1 + \psi B(t)} \right), \quad (3.4)$$

where P_{\min} and P_{\max} are the minimum and maximum self-renewal probabilities and $B(t)$ represents the concentration of BMP4. P_{\max} is attained if there is no BMP4 present, while P_{\min} is approached as $B \rightarrow \infty$. We do not consider any endogenous production of BMP4 (or other differentiation promoter), therefore it is only present during differentiation therapy. The parameter ψ represents the sensitivity of GSCs to BMP4, as ψ increases (for the same concentration of BMP4) P_{\min} is approached faster. Any other potential effects of BMP4, for example on growth rates, are ignored as they are in (Youssefpour et al. 2012) and (Bachman and Hillen 2013).

3.2.2.3 Radiotherapy model

We model the effects of radiotherapy using the linear quadratic (LQ) model, which is widely used in mathematical modelling of RT (R. Rockne et al. 2010; R. Rockne et al. 2009; O'Rourke, McAneney, and Hillen 2009; McMahon 2018). The fraction of cells that survive, $\gamma_{\text{rad}}(d)$ after a single fractional dose of, d Grays (Gy) of radiation is given by

$$\gamma_{\text{rad}}(d) = \exp(-\eta\mu(\alpha d + \beta d^2)), \quad (3.5)$$

where α can be interpreted as death from single-stranded breaks (linear component) and β can be interpreted as death from double-strand breaks (quadratic component). It has been shown that the value of α correlates with the proliferation rate of the tumor. We can use this linear relationship to estimate α on a patient-specific level as $\alpha = 0.05m_v$ (R. Rockne et al. 2010). To account for the fact that GSCs are less sensitive to radiation than other cancer cells, we include the additional radio-protection parameter η . Previous experiments have estimated GSC radio-protection to be $\eta = 0.1376$ (Gao et al. 2013; Bao et al. 2006). Additionally, the model contains cells that are terminally differentiated and so do not proliferate. RT primarily targets actively proliferating cells so is less effective against non-proliferating cells. We include μ to account for this radio-protection of non-proliferating cells, previous experiments have found this to be around $\mu = 0.5$ (Gao et al. 2013; Griffin 2006; Potten 1981).

It is assumed that all effects of radiation on tumor cell density are instantaneous, and no delay or otherwise toxic effects of radiotherapy are considered. Nor are any effects on proliferation rate as a result of radiotherapy considered. Therefore, we model the effects of radiotherapy as an instantaneous reduction of tumor density. Considering each compartment of the model (Equation 3.2) separately we modify them by

$$\begin{aligned}
s_{\text{post-rad}} &= s_{\text{pre-rad}} \exp(-\eta(\alpha d + \beta d^2)) \\
v_{i_{\text{post-rad}}} &= v_{i_{\text{pre-rad}}} \exp(-(\alpha d + \beta d^2)) \\
v_{n_{\text{post-rad}}} &= v_{n_{\text{pre-rad}}} \exp(-\mu(\alpha d + \beta d^2))
\end{aligned} \tag{3.6}$$

3.2.2.4 Resection model

Similarly to radiotherapy we model resection as an instantaneous loss of density, applied to each model compartment separately as

$$\begin{aligned}
s_{\text{post-resect}} &= s_{\text{pre-resect}} \gamma_{\text{res}} \\
v_{i_{\text{post-resect}}} &= v_{i_{\text{pre-resect}}} \gamma_{\text{res}} \\
v_{n_{\text{post-resect}}} &= v_{n_{\text{pre-resect}}} \gamma_{\text{res}},
\end{aligned} \tag{3.7}$$

where γ_{res} is the surviving fraction after resection. Chaichana et al. investigated the efficacy of resection found that on average resection resulted in a 91.7% reduction in tumor volume, so we take $\gamma_{\text{res}} = (1 - 0.917)$ ([Chaichana et al. 2014](#)).

3.3 Results

We explore the model for a range of different parameter values to help us identify possible strategies for patient selection in early phase clinical trials of BMP4 therapy, as well as explore different delivery schedules, to increase the likelihood of observing successful clinical trials. We parameterise our model to 5 GBM cell lines where we have known doubling times, radiotherapy response, and exposure to BMP4. This allows us to estimate reasonable values of sensitivity to BMP4. We develop a virtual clinical trial pipeline that allows us to assess the likelihood of observing a successful trial for different patient populations.

3.3.1 Simulating radiotherapy experiments

To parameterise the model we simulate the radiotherapy assay described in Section [3.2.1](#). In the assay a small number of cells were seeded and allowed to grow for 48hrs exposed to either CTRL (GSC media) or BMP4 (100ng/ml) then radiotherapy at 0,2,4,6 Gy was applied. The number of surviving colonies was then counted. To simulate this we initialise our model with a small density of GSCs. The cells are cultured in GSC media in the CTRL case so we assume no differentiation takes place before treatment (i.e. $P_s = 1$). We simulate the BMP4 as a constant concentration for the 48hrs. From the DLQ model (Equation [3.1](#)) we have an estimate for what the fraction of GSCs should be after the 48hrs and given that we also have the doubling time for each cell line we can fit the parameter ψ , which tells us the change in GSC self-renewal (P_s) over the 48hrs.

The fitted ψ values for each of the 5 cell lines are shown in Figure [3.2c](#) and in Table [3.1](#). We find that each cell line has a distinct sensitivity to BMP4, in agreement with work in preparation ([Farias et al., n.d.b](#))

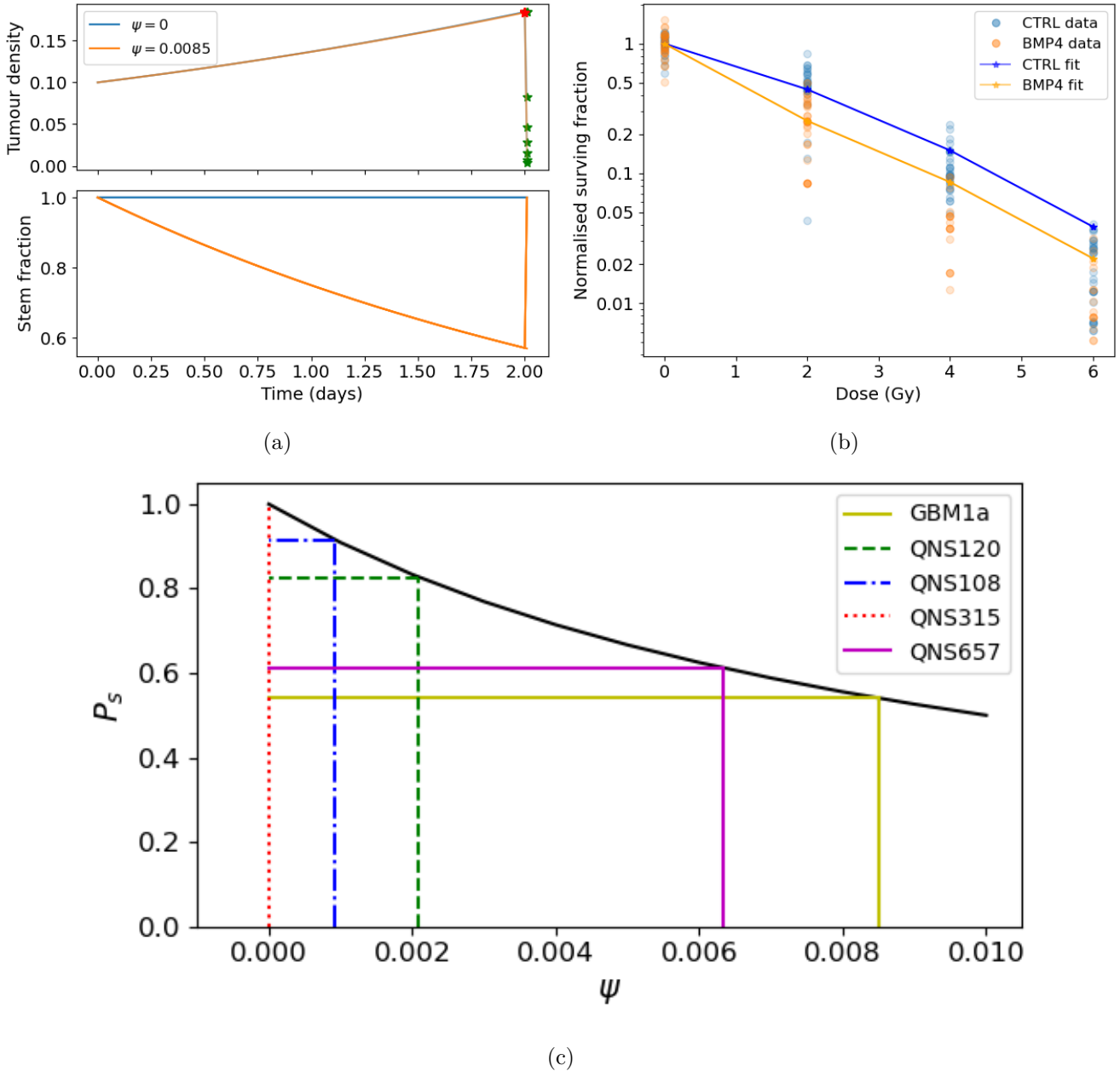


Figure 3.2: Simulated radiotherapy assay. (a) Initially a small number of cells were seeded (represented by a small density of tumor cells). These were grown for 2 days under either control or 100ng/ml BMP4. After 2 days, radiotherapy was applied at different dosages and the number of surviving colonies were counted. The red star indicates when RT was applied (48 hrs) and the green stars indicate the final measured density of tumor immediately after radiotherapy for different doses of radiation. (b) Simulated dose response to radiotherapy after fitting ψ in the ODE model to provide the expected fraction of GSCs given the doubling time of the cell line. (c) Each of the cell lines has a distinct sensitivity to BMP4 denoted ψ .

which shows that GBM1a, QNS657 and QNS120 are sensitive to BMP4 while QNS315 and QNS108 are resistant to BMP4 treatment.

Table 3.1: Fitted parameter values and metadata from cell lines. All cell lines are from primary tumor. It is assumed that $\alpha/\beta = 10$ is fixed for all cell lines.

Cell line	α	F	Doubling time (hrs)	Sensitivity to BMP4 (ψ)	Sex
GBM1a	0.338	0.571	54.7	0.00850409	Male
QNS120	0.116	0.770	43.5	0.002094342	Male
QNS108	0.151	0.949	109	0.000918066	Male
QNS315	0.0841	1	63.6	0	Female
QNS657	0.104	0.707	75.6	0.006332659	Female

3.3.2 Model simulations

We simulate our model for a range of parameter values to explore the effect of BMP4 on tumor growth. Based on our fitted values of ψ we consider a range from $[0, 0.1]$, the full parameter values are given in Table 3.2. To simulate treatment we allow the model to run until the total tumor size reaches 0.2, then initiate treatment. To evaluate the effect of BMP4, we compare two treatment arms: standard of care - resection (at the time of detection) followed by radiotherapy 30 days later, and BMP4 - standard of care with the addition of BMP4. To observe the effect of BMP4, we assume a fixed concentration of AMSCs, which release BMP4 at a constant rate, from the time of resection until the end of radiotherapy. In each case we record the number of days until the tumor reaches a size of 0.6 and refer to this as time to progression. This allows us to calculate the fold change in time to progression to directly compare for each set of parameters how much the BMP4 prolonged survival. The results are shown in Figure 3.3b.

Since GSCs are less sensitive to RT than other cells, the fraction of GSCs increases during RT; this is shown in our model in Figure 3.3a. In particular, radiotherapy is more effective against faster proliferating tumors (R. Rockne et al. 2010) so this effect is particularly pronounced in these tumors. Enrichment of GSCs during RT not only highlights that there are some resistant cells not being targeted by radiotherapy but also since these are the most tumorigenic cells, with a large proportion of GSCs, a recurrent tumor is able to form rapidly (as compared to not at all if no GSCs were present). When we simulated the addition of BMP4 (the dashed lines in Figure 3.3a) we see that this peak in stem-cell fraction is reduced due to the induced differentiation of GSCs. This means that not only is the RT more effective as there are fewer resistant GSCs but also that the tumor will take longer to recur as there are fewer GSCs to drive regrowth. As the increase in GSC fraction is most pronounced in faster proliferating tumors, we see that the relative effect of BMP4 in delaying progression is also largest for these patients.

Table 3.2: Table of parameter values used. When the value is fixed its value is given, if it is sampled from a distribution then the distribution is given.

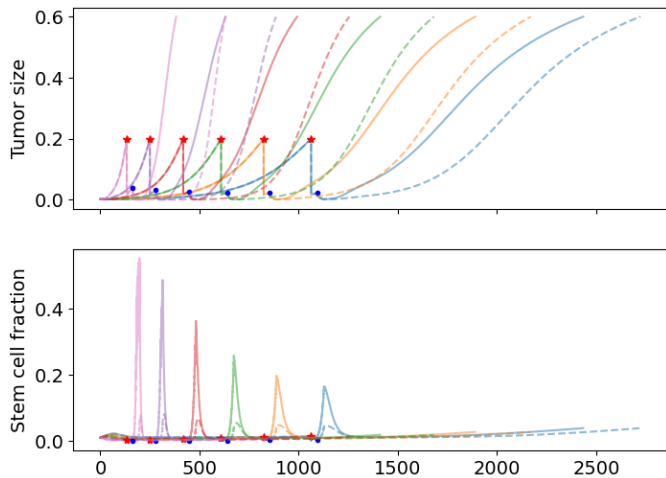
Parameter	Meaning	Value / distribution	Units	Reference
δ_s	death rate of GSCs	0.001	1 / year	Estimated
δ_i	death rate of PCs	0.01	1 / year	Estimated
δ_n	death rate of TCs	0.1	1 / year	Estimated
δ_m	death rate of AMSCs	0.5	1 / year	(Li et al. 2014b)
δ_B	Decay rate of BMP4	0.5	1 / year	(Li et al. 2014b)
u_B	Uptake rate of BMP4	0.5	1 / year	Estimated
C	Release rate of BMP4 from AMSCs	0.5	1 / year	Estimated
n	Number of division of PCs	10	-	(Gao et al. 2013)
m_i	Proliferation rate of PCs	log-N(2.75, 0.51)	1 / year	(Yang et al. 2019)
m_s	Proliferation rate of GSCs	$0.0345m_i$	1 / year	Estimated
α	Radiosensitivity	$0.05m_i$	1 / Gy	(R. Rockne et al. 2010)

3.3.3 Virtual clinical trial pipeline

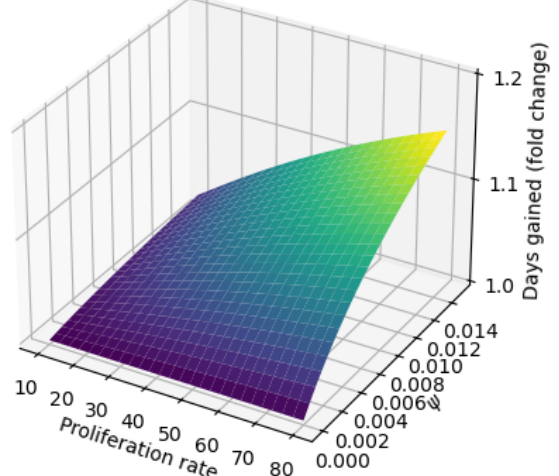
Firstly we simulate a large cohort of virtual patients with fix sensitivity to BMP4 based on the parameters identified in Section 3.3.1. We compare our simulated BMP4 patients to virtual controls to show that BMP4 can delay tumor growth. We then develop a pipeline for simulating early-phase 2 clinical trials and calculating the probability of observing a successful trial.

3.3.3.1 Uncertainty in tumor detection and death

We assume that both detection of the tumor and death depend on tumor size in a random fashion for each virtual patient. Detection (death) is more likely the bigger a tumor is, but two tumors of equal size in two patients do not necessarily lead to detection (death) at the same times. Thus, we assume that the times of tumor detection and death, represented by the random variables T_{detect} and T_{death} , depend on total tumor density $N(t)$ according to the hazard function



(a)



(b)

Figure 3.3: Effect of BMP4 on tumor progression. (a) Example model simulations showing the total tumor density and fraction of GSCs. Red stars indicate when the tumor was detected at $N = 0.2$ and the blue dot represents the start of radiotherapy (30 days later). Simulated standard of care (resection and radiotherapy) is plotted in solid lines and BMP4-AMSCs is in the dashed lines. During radiotherapy the fraction of GSCs is greatly increased as they are less sensitive than the non-GSCs. When BMP4 is added this enrichment in GSCs is reduced, delaying time for tumor regrowth. (b) Days gained surface. As we increase both the sensitivity to BMP4 (ψ) and the proliferation rate the fold change in time to progression increases.

$$P(T_d \in [t, t + \Delta t) | T_d > t) = \lambda_d(N(t))\Delta t + o(\Delta t), \quad d \in \{\text{detect, death}\}, \quad (3.8)$$

where

$$\lambda_d(N) = \frac{\lambda_{d,\max}}{1 + e^{-m_d(N - N_d)}}. \quad (3.9)$$

Here, $\lambda_d(N)$ is a shifted logistic function; $\lambda_{d,\max}$ is the maximum rate of detection that we take to be 1, m_d describes the steepness of the logistic function, which we set to be 100 in the detection case and 20 in the death case. The constant N_d is a threshold parameter at which the probability rate of detection or death is half-maximal (each of these for $d \in \{\text{detect, death}\}$), we set this to be 0.2 and 0.7 in the detection and death cases respectively. Δt is the timestep on which the model is solved numerically. This is similar to the approach of (Bartoszyński et al. 2001; Plevritis et al. 2006), apart from our choice of nonlinear dependence on tumor size. The shifted logistic function acts as a switch mechanism, meaning once $N > N_d$ the rate of detection or death rapidly increases towards its maximum. Figure 3.4a shows the form of these functions with the parameters used in the virtual trials that follow.

3.3.3.2 Simulated control virtual patient population

To construct a group of control patients, we sample proliferation rates from a distribution consistent with measured proliferation rates of around 300 patients (Yang et al. 2019), from this distribution we sample 200 patients. We then simulate these patients undergoing resection and radiotherapy (standard of care); to consider the effect of BMP4 on survival we assume a constant concentration of 100ng/ml is maintained from detection until the end of radiotherapy and we consider two different sensitivities $\psi = 0.0021$ and $\psi = 0.0085$, these values correspond with the cell lines QNS120 and GBM1a from Table 3.1. The results are shown in Figure 3.4. We see that BMP4 improves simulated survival times and that as the sensitivity to BMP4 is increased the response is more pronounced.

3.3.3.3 Simulated phase 2 trial

In practice a phase 2 trial will have only a small number of patients (typically around 20-40) and the population will be heterogeneous with respect to sensitivity to BMP4. We develop a virtual trial pipeline to consider the chance of observing a successful trial for different virtual populations. We have previously observed that proliferation rate can impact the efficacy of BMP4 treatment (Figure 3.3b). Therefore, we consider 3 stratifications of the population based on proliferation rate. We construct these by sampling twice as many virtual patients as we need for each trial (80) and then splitting them into either the top 50% fastest proliferators, the middle 50%, or the slowest 50%, so that each group has 40 virtual patients. We then split them via a stratified random split, so that both groups have similar distributions of proliferation rates, into control and treatment arms (20 in each), with parameters drawn from Table 3.2 and ψ from a truncated normal distribution. This assumes knowledge of growth rates for patients enrolled in the trial, which is straightforward for our simulated virtual patients. For each group (fast, medium, slow) we perform 20 virtual trials, each one comprising a distinct set of 40 patients, giving us an idea of the chance of observing a successful trial.

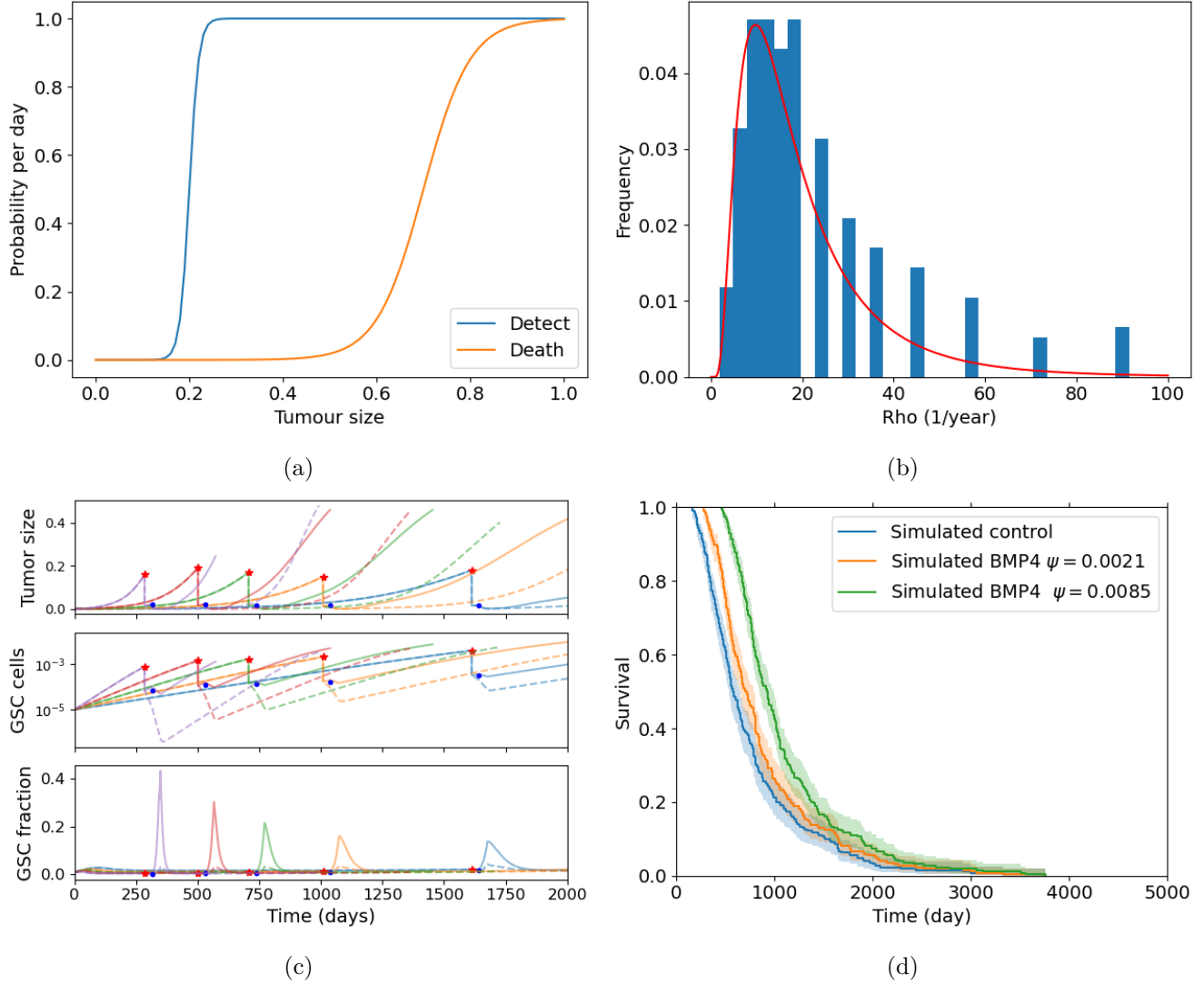


Figure 3.4: Simulated virtual control patients. (a) Tumor detection and death are considered random events which increase in probability as tumor size increases. (b) Histogram of proliferation rates from (Yang et al. 2019), red line shows fitted log normal distribution (c) Example model simulation trajectories showing overall tumor density and fraction of stem cells. The red stars indicate when the tumor was detected and the blue dots when radiotherapy was started. (d) Comparison of survival times for simulated control patients (resection and radiotherapy) with BMP4 treatment, for two different sensitivities to BMP4.

We assume a distribution of sensitivities drawn from a truncated normal distribution with mean sensitivity $\psi_{\text{mean}} = 0.0085$, so that, according to our model fits this would be a population that has been identified as highly sensitive to BMP4. For this cohort of virtual patients we consider a possible delivery schedule of BMP4-AMSCs which we shall term ‘single-hit’, this consists of a single dose of AMSCs-BMP4 at the time of resection. This is a promising and practical option for BMP4-AMSCs delivery as they can be implanted directly into the tumor at the time of resection and means the patient is receiving some treatment in the time between resection and radiotherapy, when typically they receive none during this time. For this cohort of virtual patients, we implement a series of different concentrations of AMSCs-BMP4; in Figure 3.5 we show average BMP4 concentration in ng/ml, to compare this to the radiotherapy assay in Section 3.3.1. An average concentration of 8ng/ml corresponds to a peak of 100ng/ml at the time of resection, the same concentration maintained for two days in the assay. We see that, for peak concentrations of BMP4 similar to that in the *in vitro* assay, no trials show statistically significant differences in survival curves (log-rank test, $p > 0.05$). Indeed, according to these results a considerably higher total dose of BMP4 is required in order to see consistently successful trials (defined as rejecting the null hypothesis of identical survival curves between control and treatment arms). This may be because of the relatively rapid decay of AMSCs and BMP4; if AMSCs are delivered at the time of resection very few remain and BMP4 concentrations are low by the time RT begins.

The results plotted in Figure 3.5 are for the group of fast proliferators only as this was the only group which saw a significant response to BMP4 therapy. Figure 3.5d shows a summary of the results for all the proliferation groups. This highlights the importance of considering other patient specific parameters when selecting potential patients for clinical trial.

3.3.3.4 Different delivery schedules for BMP4

The high concentrations of BMP4 required in a single-hit approach identified in Section 3.3.3.3 motivates us to look at alternative dosing strategies, where similar or greater benefit may be observed for less average dose of BMP4. As the AMSCs only last for around 2 weeks (and BMP4 slightly less) only a small concentration is left by the time radiotherapy occurs in the single-hit approach. Since BMP4 increases the radiosensitivity of the tumor and reduces the enrichment of GSCs when radiotherapy occurs, delivering it in combination with radiotherapy may provide significantly improved responses even when a similar total dose of BMP4 is considered. Therefore, we consider 3 alternative treatment schedules: i) a single dose immediately before radiotherapy, ii) a continuous dose from resection until the end of RT and iii) periodic doses in combination with radiotherapy. These schedules are shown in Figure 3.6a. In all cases, the same total dose of BMP4 (this corresponds to the same area under the curve in Figure 3.6a) will be administered so the comparison is fair between delivery schedules.

We use the same virtual trial pipeline outlined previously in Section 3.3.3, applied to these three alternative dosing strategies. A summary of the results for the fast proliferating group is plotted in Figure 3.6b. We see that the continuous delivery schedule is the most effective, with the highest number of successful trials with an average BMP4 concentration of around 10ng/ml required for almost all trials to be successful. This is closely followed by the periodic schedule. The shifted single dose appears to be largely similar in efficacy as the single dose at resection. These show that longer term exposure of BMP4 greatly increases its efficacy. This highlights the importance of designing the delivery schedule of BMP4 to maximise the effect of the treatment, and in future could be optimised on a patient-specific level.

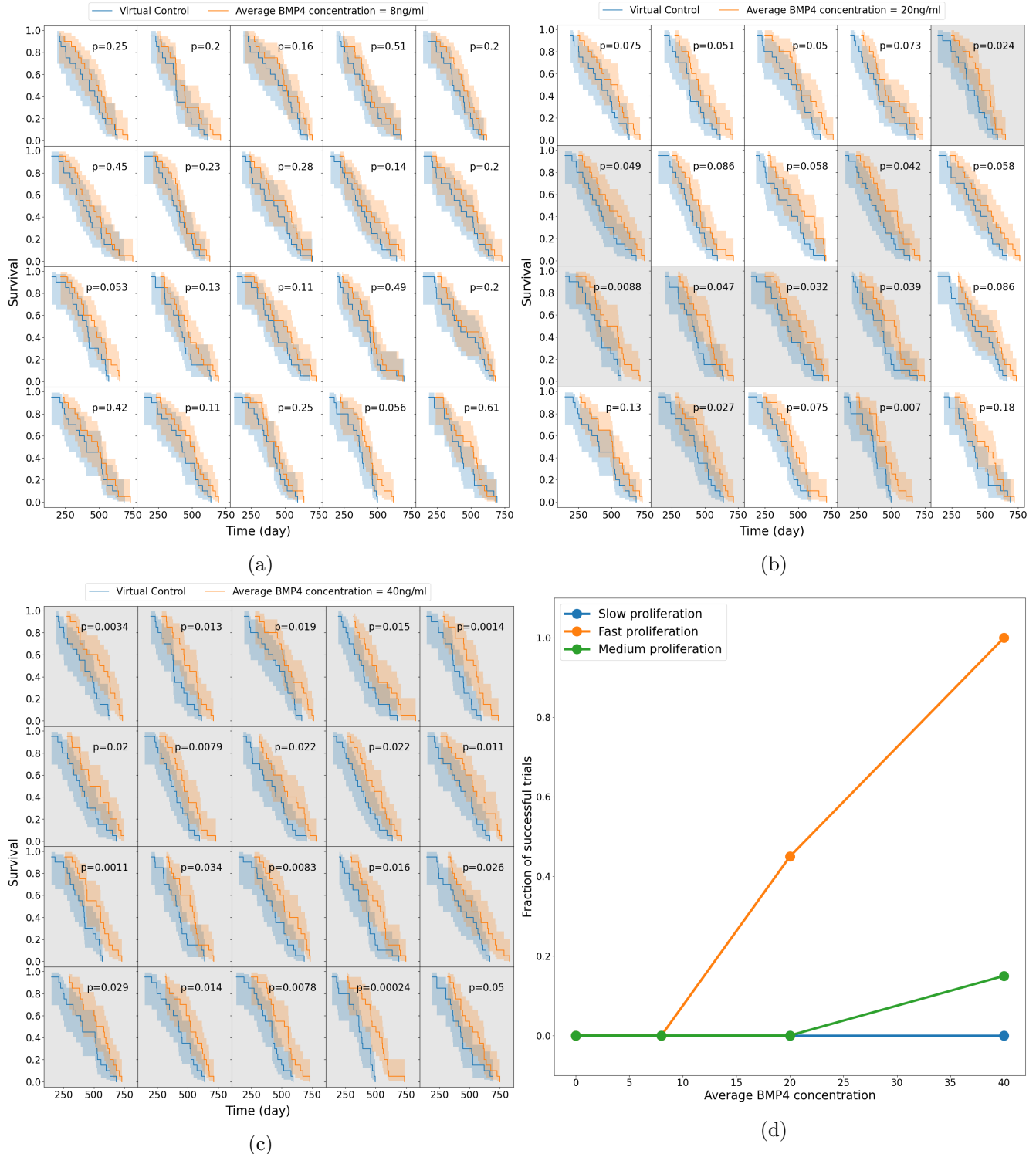


Figure 3.5: Survival curves for 20 simulated virtual trials for the fast proliferating stratification shaded by success (if BMP4 treatment arm is significantly different to the control arm) for four different concentrations of BMP4. (a) As expected, when BMP4 is low the control and treatment arms are similar in all 20 trials. (b) As BMP4 concentration increases, the fraction of successful trials increases. (c) For sufficiently high BMP4 (and hence a sufficiently strong treatment effect), almost all trials are successful. (d) Summary of the successful trial from phase 2. Orange, green and blue represent fast, medium and slow proliferation, respectively.

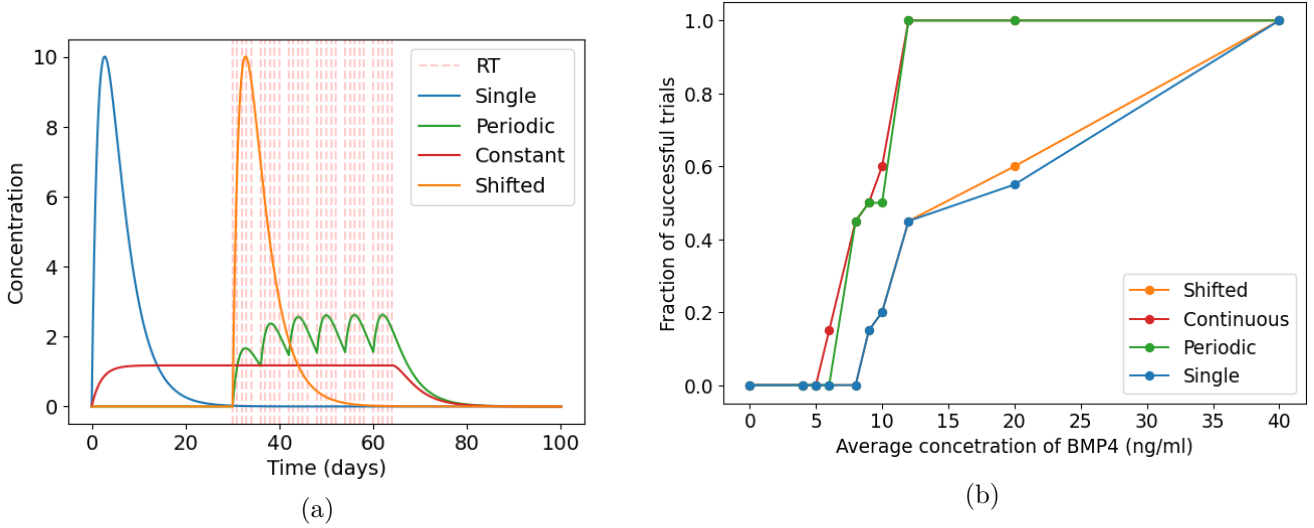


Figure 3.6: Alternative delivery schedules have improved response to BMP4 for same total dose. (a) Different delivery schedules for BMP4. Here time 0 represents the time of detection and radiotherapy occurs 30 days after detection. (b) Summary of fraction of successful trials for different delivery schedules.

3.4 Discussion

In this study, we have developed a comprehensive mathematical model to simulate GSC-driven tumor growth, specifically focusing on the impact of BMP4 treatment. By parameterizing our model using experimental data from five distinct glioma stem cell lines exposed to BMP4, we were able to qualitatively estimate the sensitivity of these cell lines to BMP4. This approach provides valuable insights into the potential variability in treatment response among different glioma cell populations.

A key limitation of our model lies in the inherent assumptions necessary for reducing the complex biology of glioblastoma/glioma to a system of ordinary differential equations (ODEs). While our model successfully encapsulates many aspects of tumor dynamics, it does not explicitly account for the spatial heterogeneity of glioblastoma. Future work could expand this model to incorporate spatial considerations, to better capture the intricate microenvironment and its influence on tumor behaviour. That said, we hope that capturing the essence of the proposed BMP4 treatment in the current model has highlighted key mechanisms by which impact on tumor growth may or may not be seen in the clinic.

Moreover, our study primarily concentrated on the impact of BMP4-induced differentiation on radiosensitivity, leaving the direct effects of BMP4 on proliferation rates as an area for further exploration. Understanding how BMP4 modulates proliferation, in addition to differentiation, could provide a more comprehensive picture of its therapeutic potential and guide the development of more effective treatment strategies.

Importantly, we have also demonstrated a virtual clinical trial pipeline to evaluate the potential of BMP4-AMSCs treatment for patients with GBM. Our simulations revealed that a significant amount of BMP4

would be required to achieve successful outcomes in a substantial proportion of patients. This finding underscores the importance of optimizing BMP4 dosage and delivery methods for future clinical applications. Additionally, our results suggest that patient stratification based on proliferation rates could enhance the likelihood of treatment success. By selecting patients with higher proliferation rates, we could potentially increase the observed efficacy of BMP4 in combination with radiotherapy.

Furthermore, we explored various BMP4 delivery schedules and identified that alternative strategies could enhance the therapeutic synergy between BMP4 and radiotherapy. These findings indicate that the timing and duration of BMP4 administration, in particular in relation to the timing of radiotherapy, can be crucial factors that could be optimized to improve clinical outcomes. We have shown that prolonged exposure to BMP4 greatly increased its efficacy when compared to a 'single-hit' approach. Future studies could expand on this by investigating different delivery modalities and schedules, potentially in combination with other therapies, to maximize the therapeutic benefit of BMP4.

In conclusion, our work provides a robust framework for virtual clinical trials, offering valuable predictions that can guide the clinical translation of BMP4-based therapies for GBM. By highlighting the need for high BMP4 levels, patient stratification, and optimized delivery strategies, we have laid the groundwork for future studies that can further refine and validate these approaches in a clinical context.

References

Acar, Ahmet, Daniel Nichol, Javier Fernandez-Mateos, George D. Cresswell, Iros Barozzi, Sung Pil Hong, Nicholas Trahearn, et al. 2020. “Exploiting Evolutionary Steering to Induce Collateral Drug Sensitivity in Cancer.” *Nature Communications* 11 (1): 1923. <https://doi.org/10.1038/s41467-020-15596-z>.

Al-Hajj, Muhammad, Max S. Wicha, Adalberto Benito-Hernandez, Sean J. Morrison, and Michael F. Clarke. 2003. “Prospective Identification of Tumorigenic Breast Cancer Cells.” *Proceedings of the National Academy of Sciences* 100 (7): 3983–88. <https://doi.org/10.1073/pnas.0530291100>.

Bachman, Jeff W. N., and Thomas Hillen. 2013. “Mathematical Optimization of the Combination of Radiation and Differentiation Therapies for Cancer.” *Frontiers in Oncology* 3. <https://doi.org/10.3389/fonc.2013.00052>.

Bagley, Stephen J., Shawn Kothari, Rifaquat Rahman, Eudocia Q. Lee, Gavin P. Dunn, Evanthia Galanis, Susan M. Chang, et al. 2022. “Glioblastoma Clinical Trials: Current Landscape and Opportunities for Improvement.” *Clinical Cancer Research* 28 (4): 594–602. <https://doi.org/10.1158/1078-0432.CCR-21-2750>.

Bailey, Jennifer M., Pankaj K. Singh, and Michael A. Hollingsworth. 2007. “Cancer Metastasis Facilitated by Developmental Pathways: Sonic Hedgehog, Notch, and Bone Morphogenic Proteins.” *Journal of Cellular Biochemistry* 102 (4): 829–39. <https://doi.org/10.1002/jcb.21509>.

Balk, Sophie J. 2011. “Ultraviolet Radiation: A Hazard to Children and Adolescents.” *Pediatrics* 127 (3): e791–817. <https://doi.org/10.1542/peds.2010-3502>.

Bao, Shideng, Qulian Wu, Roger E. McLendon, Yueling Hao, Qing Shi, Anita B. Hjelmeland, Mark W. Dewhirst, Darell D. Bigner, and Jeremy N. Rich. 2006. “Glioma Stem Cells Promote Radioresistance by Preferential Activation of the DNA Damage Response.” *Nature* 444 (7120): 756–60. <https://doi.org/10.1038/nature05236>.

Bartoszyński, Robert, Lutz Edler, Leonid Hanin, Annette Kopp-Schneider, Lyudmila Pavlova, Alexander Tsodikov, Alexander Zorin, and Andrej Yu. Yakovlev. 2001. “Modeling Cancer Detection: Tumor Size as a Source of Information on Unobservable Stages of Carcinogenesis.” *Mathematical Biosciences* 171 (2): 113–42. [https://doi.org/10.1016/s0025-5564\(01\)00058-x](https://doi.org/10.1016/s0025-5564(01)00058-x).

Baskar, Rajamanickam, Kuo Ann Lee, Richard Yeo, and Kheng-Wei Yeoh. 2012. “Cancer and Radiation Therapy: Current Advances and Future Directions.” *International Journal of Medical Sciences* 9 (3): 193–99. <https://doi.org/10.7150/ijms.3635>.

Bonnet, Dominique, and John E. Dick. 1997. “Human Acute Myeloid Leukemia Is Organized as a Hierarchy That Originates from a Primitive Hematopoietic Cell.” *Nature Medicine* 3 (7): 730–37. <https://doi.org/10.1038/nm0797-730>.

Breward, C. 2003. “A Multiphase Model Describing Vascular Tumour Growth.” *Bulletin of Mathematical Biology* 65 (4): 609–40. [https://doi.org/10.1016/S0092-8240\(03\)00027-2](https://doi.org/10.1016/S0092-8240(03)00027-2).

Cardinal, Olivia, Chloé Burlot, Yangxin Fu, Powel Crosley, Mary Hitt, Morgan Craig, and Adrienne L. Jenner. 2022. “Establishing Combination PAC-1 and TRAIL Regimens for Treating Ovarian Cancer Based on Patient-Specific Pharmacokinetic Profiles Using *in Silico* Clinical Trials.” *Computational and Systems Oncology* 2 (2). <https://doi.org/10.1002/cso2.1035>.

Carén, Helena, Stephan Beck, and Steven M. Pollard. 2016. "Differentiation Therapy for Glioblastoma – Too Many Obstacles?" *Molecular & Cellular Oncology* 3 (2): e1124174. <https://doi.org/10.1080/23723556.2015.1124174>.

Chaichana, Kaisorn L., Eibar Ernesto Cabrera-Aldana, Ignacio Jusue-Torres, Olindi Wijesekera, Alessandro Olivi, Maryam Rahman, and Alfredo Quinones-Hinojosa. 2014. "When Gross Total Resection of a Glioblastoma Is Possible, How Much Resection Should Be Achieved?" *World Neurosurgery* 82 (1-2): e257–65. <https://doi.org/10.1016/j.wneu.2014.01.019>.

Cloughesy, Timothy F., Kevin Petrecca, Tobias Walbert, Nicholas Butowski, Michael Salacz, James Perry, Denise Damek, et al. 2020. "Effect of Vocimagene Amiretrorepvec in Combination With Flucytosine Vs Standard of Care on Survival Following Tumor Resection in Patients With Recurrent High-Grade Glioma: A Randomized Clinical Trial." *JAMA Oncology* 6 (12): 1939. <https://doi.org/10.1001/jamaoncol.2020.3161>.

Craig, Morgan, Jana L. Gevertz, Irina Kareva, and Kathleen P. Wilkie. 2023. "A Practical Guide for the Generation of Model-Based Virtual Clinical Trials." *Frontiers in Systems Biology* 3 (June). <https://doi.org/10.3389/fsysb.2023.1174647>.

De Thé, Hugues. 2018. "Differentiation Therapy Revisited." *Nature Reviews Cancer* 18 (2): 117–27. <https://doi.org/10.1038/nrc.2017.103>.

Dingli, David, and Franziska Michor. 2006. "Successful Therapy Must Eradicate Cancer Stem Cells." *STEM CELLS* 24 (12): 2603–10. <https://doi.org/10.1634/stemcells.2006-0136>.

Dirks, Peter B. 2006. "Stem Cells and Brain Tumours." *Nature* 444 (7120): 687–88. <https://doi.org/10.1038/444687a>.

Doucette, Tiffany, Ganesh Rao, Yuhui Yang, Joy Gumin, Naoki Shinojima, B. Nebyou Bekele, Wei Qiao, Wei Zhang, and Frederick F. Lang. 2011. "Mesenchymal Stem Cells Display Tumor-Specific Tropism in an RCAS/Ntv-a Glioma Model." *Neoplasia* 13 (8): 716–25. <https://doi.org/10.1593/neo.101680>.

Dowden, Helen, and Jamie Munro. 2019. "Trends in Clinical Success Rates and Therapeutic Focus." *Nature Reviews Drug Discovery* 18 (7): 495–96. <https://doi.org/10.1038/d41573-019-00074-z>.

Enderling, Heiko, Alexander R. A. Anderson, Mark A. J. Chaplain, Afshin Beheshti, Lynn Hlatky, and Philip Hahnfeldt. 2009. "Paradoxical Dependencies of Tumor Dormancy and Progression on Basic Cell Kinetics." *Cancer Research* 69 (22): 8814–21. <https://doi.org/10.1158/0008-5472.CAN-09-2115>.

Enriquez-Navas, Pedro M., Jonathan W. Wojtkowiak, and Robert A. Gatenby. 2015. "Application of Evolutionary Principles to Cancer Therapy." *Cancer Research* 75 (22): 4675–80. <https://doi.org/10.1158/0008-5472.CAN-15-1337>.

Farias, Virginia, Vinitha Rani, Natanael Zacro, Mieu Brooks, Naveen Nagaiah, Henry Ruiz-Garcia, Rachel Sarabia-Estrada, et al. n.d.b. "BMP4-Secreting MSCs Derived from Human Adipose Tissue Radiosensitize Glioblastoma Stem Cells via Downregulation of OLIG2 Signaling Pathway." *In Preparation*.

———, et al. n.d.a. "BMP4-Secreting MSCs Derived from Human Adipose Tissue Radiosensitize Glioblastoma Stem Cells via Downregulation of OLIG2 Signaling Pathway." *In Preparation*.

Folkman, Judah, and Raghu Kalluri. 2004. "Cancer Without Disease." *Nature* 427 (6977): 787–87. <https://doi.org/10.1038/427787a>.

Galli, Rossella, Elena Binda, Ugo Orfanelli, Barbara Cipelletti, Angela Gritti, Simona De Vitis, Roberta Fiocco, Chiara Foroni, Francesco Dimeco, and Angelo Vescovi. 2004. "Isolation and Characterization of Tumorigenic, Stem-Like Neural Precursors from Human Glioblastoma." *Cancer Research* 64 (19): 7011–21. <https://doi.org/10.1158/0008-5472.CAN-04-1364>.

Gao, Xuefeng, J. Tyson McDonald, Lynn Hlatky, and Heiko Enderling. 2013. "Acute and Fractionated Irradiation Differentially Modulate Glioma Stem Cell Division Kinetics." *Cancer Research* 73 (5): 1481–90. <https://doi.org/10.1158/0008-5472.CAN-12-3429>.

Griffin, Robert J. 2006. "Radiobiology for the Radiologist, 6th Edition." *International Journal of Radiation Oncology*Biology*Physics* 66 (2): 627. <https://doi.org/10.1016/j.ijrobp.2006.06.027>.

Guerrero-Cázares, Hugo, Stephany Y. Tzeng, Noah P. Young, Ameer O. Abutaleb, Alfredo Quiñones-Hinojosa, and Jordan J. Green. 2014. "Biodegradable Polymeric Nanoparticles Show High Efficacy and Specificity at DNA Delivery to Human Glioblastoma *in Vitro* and *in Vivo*." *ACS Nano* 8 (5): 5141–53. <https://doi.org/10.1021/nn501197v>.

Hanahan, Douglas, and Robert A Weinberg. 2000. "The Hallmarks of Cancer." *Cell* 100 (1): 57–70. [https://doi.org/10.1016/S0092-8674\(00\)81683-9](https://doi.org/10.1016/S0092-8674(00)81683-9).

Hemmati, Houman D., Ichiro Nakano, Jorge A. Lazareff, Michael Masterman-Smith, Daniel H. Geschwind, Marianne Bronner-Fraser, and Harley I. Kornblum. 2003. "Cancerous Stem Cells Can Arise from Pediatric Brain Tumors." *Proceedings of the National Academy of Sciences* 100 (25): 15178–83. <https://doi.org/10.1073/pnas.2036535100>.

Hillen, Thomas, Heiko Enderling, and Philip Hahnfeldt. 2013. "The Tumor Growth Paradox and Immune System-Mediated Selection for Cancer Stem Cells." *Bulletin of Mathematical Biology* 75 (1): 161–84. <https://doi.org/10.1007/s11538-012-9798-x>.

Hitomi, Masahiro, Anastasia P. Chumakova, Daniel J. Silver, Arnon M. Knudsen, W. Dean Pontius, Stephanie Murphy, Neha Anand, Bjarne W. Kristensen, and Justin D. Lathia. 2021a. "Asymmetric Cell Division Promotes Therapeutic Resistance in Glioblastoma Stem Cells." *JCI Insight* 6 (3): e130510. <https://doi.org/10.1172/jci.insight.130510>.

———. 2021b. "Asymmetric Cell Division Promotes Therapeutic Resistance in Glioblastoma Stem Cells." *JCI Insight* 6 (3): e130510. <https://doi.org/10.1172/jci.insight.130510>.

Hubbard, M. E., and H. M. Byrne. 2013. "Multiphase Modelling of Vascular Tumour Growth in Two Spatial Dimensions." *Journal of Theoretical Biology* 316 (January): 70–89. <https://doi.org/10.1016/j.jtbi.2012.09.031>.

Ignatova, Tatyana N., Valery G. Kukekov, Eric D. Laywell, Oleg N. Suslov, Frank D. Vrionis, and Dennis A. Steindler. 2002. "Human Cortical Glial Tumors Contain Neural Stem-Like Cells Expressing Astroglial and Neuronal Markers in Vitro." *Glia* 39 (3): 193–206. <https://doi.org/10.1002/glia.10094>.

Kim, Eunjung, Vito W. Rebecca, Keiran S. M. Smalley, and Alexander R. A. Anderson. 2016. "Phase i Trials in Melanoma: A Framework to Translate Preclinical Findings to the Clinic." *European Journal of Cancer* 67 (November): 213–22. <https://doi.org/10.1016/j.ejca.2016.07.024>.

Kim, Jayoung, Sujan K. Mondal, Stephany Y. Tzeng, Yuan Rui, Rawan Al-kharboosh, Kristen K. Kozielski, Adip G. Bhargav, Cesar A. Garcia, Alfredo Quiñones-Hinojosa, and Jordan J. Green. 2020. "Poly(ethylene Glycol)-Poly(beta-Amino Ester)-Based Nanoparticles for Suicide Gene Therapy Enhance Brain Penetration and Extend Survival in a Preclinical Human Glioblastoma Orthotopic Xenograft Model." *ACS Biomaterials Science & Engineering* 6 (5): 2943–55. <https://doi.org/10.1021/acsbiomaterials.0c00116>.

Lander, Arthur D, Kimberly K Gokoffski, Frederic Y. M Wan, Qing Nie, and Anne L Calof. 2009. "Cell Lineages and the Logic of Proliferative Control." Edited by Charles F Stevens. *PLoS Biology* 7 (1): e1000015. <https://doi.org/10.1371/journal.pbio.1000015>.

Lapidot, Tsvee, Christian Sirard, Josef Vormoor, Barbara Murdoch, Trang Hoang, Julio Caceres-Cortes, Mark Minden, Bruce Paterson, Michael A. Caligiuri, and John E. Dick. 1994. "A Cell Initiating Human Acute Myeloid Leukaemia After Transplantation into SCID Mice." *Nature* 367 (6464): 645–48. <https://doi.org/10.1038/367645a0>.

Lathia, J D, M Hitomi, J Gallagher, S P Gadani, J Adkins, A Vasanji, L Liu, et al. 2011. "Distribution of CD133 Reveals Glioma Stem Cells Self-Renew Through Symmetric and Asymmetric Cell Divisions." *Cell Death & Disease* 2 (9): e200–200. <https://doi.org/10.1038/cddis.2011.80>.

Lee, Yeri, Jin-Ku Lee, Sun Hee Ahn, Jeongwu Lee, and Do-Hyun Nam. 2016. "WNT Signaling in Glioblastoma and Therapeutic Opportunities." *Laboratory Investigation* 96 (2): 137–50. <https://doi.org/10.1038/labinvest.2015.140>.

Li, Qian, Olindi Wijesekera, Sussan J. Salas, Joanna Y. Wang, Mingxin Zhu, Colette Aprhys, Kaisorn L. Chaichana, et al. 2014b. "Mesenchymal Stem Cells from Human Fat Engineered to Secrete BMP4 Are Nononcogenic, Suppress Brain Cancer, and Prolong Survival." *Clinical Cancer Research* 20 (9): 2375–87. <https://doi.org/10.1158/1078-0432.CCR-13-1415>.

_____, et al. 2014a. "Mesenchymal Stem Cells from Human Fat Engineered to Secrete BMP4 Are Nononcogenic, Suppress Brain Cancer, and Prolong Survival." *Clinical Cancer Research* 20 (9): 2375–87. <https://doi.org/10.1158/1078-0432.CCR-13-1415>.

Lowengrub, J S, H B Frieboes, F Jin, Y-L Chuang, X Li, P Macklin, S M Wise, and V Cristini. 2010. "Nonlinear Modelling of Cancer: Bridging the Gap Between Cells and Tumours." *Nonlinearity* 23 (1): R1–91. <https://doi.org/10.1088/0951-7715/23/1/R01>.

Ma, Qianquan, Wenyong Long, Changsheng Xing, Junjun Chu, Mei Luo, Helen Y. Wang, Qing Liu, and Rong-Fu Wang. 2018. "Cancer Stem Cells and Immunosuppressive Microenvironment in Glioma." *Frontiers in Immunology* 9 (December): 2924. <https://doi.org/10.3389/fimmu.2018.02924>.

Majumdar, Sreemita, and Song-Tao Liu. 2020. "Cell Division Symmetry Control and Cancer Stem Cells." *AIMS Molecular Science* 7 (2): 82–101. <https://doi.org/10.3934/molsci.2020006>.

Mangraviti, Antonella, Stephany Y. Tzeng, David Gullotti, Kristen L. Kozielski, Jennifer E. Kim, Michael Seng, Sara Abbadi, et al. 2016b. "Non-Virally Engineered Human Adipose Mesenchymal Stem Cells Produce BMP4, Target Brain Tumors, and Extend Survival." *Biomaterials* 100 (September): 53–66. <https://doi.org/10.1016/j.biomaterials.2016.05.025>.

_____, et al. 2016a. "Non-Virally Engineered Human Adipose Mesenchymal Stem Cells Produce BMP4, Target Brain Tumors, and Extend Survival." *Biomaterials* 100 (September): 53–66. <https://doi.org/10.1016/j.biomaterials.2016.05.025>.

McMahon, Stephen Joseph. 2018. "The Linear Quadratic Model: Usage, Interpretation and Challenges." *Physics in Medicine & Biology* 64 (1): 01TR01. <https://doi.org/10.1088/1361-6560/aaf26a>.

Meza, Rafael, Jihyoun Jeon, Suresh H. Moolgavkar, and E. Georg Luebeck. 2008. "Age-Specific Incidence of Cancer: Phases, Transitions, and Biological Implications." *Proceedings of the National Academy of Sciences* 105 (42): 16284–89. <https://doi.org/10.1073/pnas.0801151105>.

Narita, Yoshitaka, Yoshiki Arakawa, Fumiyuki Yamasaki, Ryo Nishikawa, Tomokazu Aoki, Masayuki Kanamori, Motoo Nagane, et al. 2019. "A Randomized, Double-Blind, Phase III Trial of Personalized Peptide Vaccination for Recurrent Glioblastoma." *Neuro-Oncology* 21 (3): 348–59. <https://doi.org/10.1093/neuonc/noy200>.

Nayak, Sonali, Ashorne Mahenthiran, Yongyong Yang, Mark McClendon, Barbara Mania-Farnell, Charles David James, John A. Kessler, et al. 2020. "Bone Morphogenetic Protein 4 Targeting Glioma Stem-Like Cells for Malignant Glioma Treatment: Latest Advances and Implications for Clinical Application." *Cancers* 12 (2): 516. <https://doi.org/10.3390/cancers12020516>.

Neves-E-Castro, Manuel. 2006. "Why Do Some Breast Cancer Cells Remain Dormant?" *Gynecological Endocrinology* 22 (4): 190–97. <https://doi.org/10.1080/09513590600624374>.

O'Rourke, S. F. C., H. McAneney, and T. Hillen. 2009. "Linear Quadratic and Tumour Control Probability Modelling in External Beam Radiotherapy." *Journal of Mathematical Biology* 58 (4-5): 799–817. <https://doi.org/10.1007/s00285-008-0222-y>.

Ostrom, Quinn T, Gino Ciolfi, Haley Gittleman, Nirav Patil, Kristin Waite, Carol Kruchko, and Jill S Barnholtz-Sloan. 2019. "CBTRUS Statistical Report: Primary Brain and Other Central Nervous System Tumors Diagnosed in the United States in 2012–2016." *Neuro-Oncology* 21 (Supplement_5):

v1–100. <https://doi.org/10.1093/neuonc/noz150>.

Pannuti, Antonio, Kimberly Foreman, Paola Rizzo, Clodia Osipo, Todd Golde, Barbara Osborne, and Lucio Miele. 2010. “Targeting Notch to Target Cancer Stem Cells.” *Clinical Cancer Research* 16 (12): 3141–52. <https://doi.org/10.1158/1078-0432.CCR-09-2823>.

Pendleton, Courtney, Qian Li, David A. Chesler, Kristy Yuan, Hugo Guerrero-Cazares, and Alfredo Quinones-Hinojosa. 2013b. “Mesenchymal Stem Cells Derived from Adipose Tissue Vs Bone Marrow: In Vitro Comparison of Their Tropism Towards Gliomas.” Edited by Joseph Najbauer. *PLoS ONE* 8 (3): e58198. <https://doi.org/10.1371/journal.pone.0058198>.

———. 2013a. “Mesenchymal Stem Cells Derived from Adipose Tissue Vs Bone Marrow: In Vitro Comparison of Their Tropism Towards Gliomas.” Edited by Joseph Najbauer. *PLoS ONE* 8 (3): e58198. <https://doi.org/10.1371/journal.pone.0058198>.

Piccirillo, S. G. M., B. A. Reynolds, N. Zanetti, G. Lamorte, E. Binda, G. Broggi, H. Brem, A. Olivi, F. Dimeco, and A. L. Vescovi. 2006. “Bone Morphogenetic Proteins Inhibit the Tumorigenic Potential of Human Brain Tumour-Initiating Cells.” *Nature* 444 (7120): 761–65. <https://doi.org/10.1038/nature05349>.

Plevritis, Sylvia K., Peter Salzman, Bronislava M. Sigal, and Peter W. Glynn. 2006. “A Natural History Model of Stage Progression Applied to Breast Cancer.” *Statistics in Medicine* 26 (3): 581–95. <https://doi.org/10.1002/sim.2550>.

Potten, C. S. 1981. “The Cell Kinetic Mechanism for Radiation-Induced Cellular Depletion of Epithelial Tissue Based on Hierarchical Differences in Radiosensitivity.” *International Journal of Radiation Biology and Related Studies in Physics, Chemistry and Medicine* 40 (2): 217–25. <https://doi.org/10.1080/09553008114551101>.

Reardon, David A., Alba A. Brandes, Antonio Omuro, Paul Mulholland, Michael Lim, Antje Wick, Joachim Baehring, et al. 2020. “Effect of Nivolumab Vs Bevacizumab in Patients With Recurrent Glioblastoma: The CheckMate 143 Phase 3 Randomized Clinical Trial.” *JAMA Oncology* 6 (7): 1003. <https://doi.org/10.1001/jamaoncol.2020.1024>.

Reya, Tannishtha, Sean J. Morrison, Michael F. Clarke, and Irving L. Weissman. 2001. “Stem Cells, Cancer, and Cancer Stem Cells.” *Nature* 414 (6859): 105–11. <https://doi.org/10.1038/35102167>.

Ricci-Vitiani, Lucia, Dario G. Lombardi, Emanuela Pilozzi, Mauro Biffoni, Matilde Todaro, Cesare Peschle, and Ruggero De Maria. 2007. “Identification and Expansion of Human Colon-Cancer-Initiating Cells.” *Nature* 445 (7123): 111–15. <https://doi.org/10.1038/nature05384>.

Rich, Jeremy N. 2007. “Cancer Stem Cells in Radiation Resistance.” *Cancer Research* 67 (19): 8980–84. <https://doi.org/10.1158/0008-5472.CAN-07-0895>.

Rockne, R., E. C. Alvord, J. K. Rockhill, and K. R. Swanson. 2009. “A Mathematical Model for Brain Tumor Response to Radiation Therapy.” *Journal of Mathematical Biology* 58 (4-5): 561. <https://doi.org/10.1007/s00285-008-0219-6>.

Rockne, R, J K Rockhill, M Mrugala, A M Spence, I Kalet, K Hendrickson, A Lai, T Cloughesy, E C Alvord, and K R Swanson. 2010. “Predicting the Efficacy of Radiotherapy in Individual Glioblastoma Patients *in Vivo*: A Mathematical Modeling Approach.” *Physics in Medicine and Biology* 55 (12): 3271–85. <https://doi.org/10.1088/0031-9155/55/12/001>.

Roth, Patrick, Thierry Gorlia, Jaap C. Reijneveld, Filip Yves Francine Leon De Vos, Ahmed Idbaih, Jean-Sebastien Frenel, Emilie Le Rhun, et al. 2021. “EORTC 1709/CCTG CE.8: A Phase III Trial of Marizomib in Combination with Temozolomide-Based Radiochemotherapy Versus Temozolomide-Based Radiochemotherapy Alone in Patients with Newly Diagnosed Glioblastoma.” *Journal of Clinical Oncology* 39 (15_suppl): 2004–4. https://doi.org/10.1200/JCO.2021.39.15_suppl.2004.

Schonberg, David L., Daniel Lubelski, Tyler E. Miller, and Jeremy N. Rich. 2014. “Brain Tumor Stem

Cells: Molecular Characteristics and Their Impact on Therapy.” *Molecular Aspects of Medicine* 39 (October): 82–101. <https://doi.org/10.1016/j.mam.2013.06.004>.

Sell, S. 1993. “Cellular Origin of Cancer: Dedifferentiation or Stem Cell Maturation Arrest?” *Environmental Health Perspectives* 101 (suppl 5): 15–26. <https://doi.org/10.1289/ehp.93101s515>.

Singh, Sheila K., Ian D. Clarke, Mizuhiko Terasaki, Victoria E. Bonn, Cynthia Hawkins, Jeremy Squire, and Peter B. Dirks. 2003. “Identification of a Cancer Stem Cell in Human Brain Tumors.” *Cancer Research* 63 (18): 5821–28.

Singh, Sheila K., Cynthia Hawkins, Ian D. Clarke, Jeremy A. Squire, Jane Bayani, Takuichiro Hide, R. Mark Henkelman, Michael D. Cusimano, and Peter B. Dirks. 2004. “Identification of Human Brain Tumour Initiating Cells.” *Nature* 432 (7015): 396–401. <https://doi.org/10.1038/nature03128>.

Smith, Chris L., Kaisorn L. Chaichana, Young M. Lee, Benjamin Lin, Kevin M. Stanko, Thomas O’Donnell, Saksham Gupta, et al. 2015. “Pre-Exposure of Human Adipose Mesenchymal Stem Cells to Soluble Factors Enhances Their Homing to Brain Cancer.” *Stem Cells Translational Medicine* 4 (3): 239–51. <https://doi.org/10.5966/sctm.2014-0149>.

Stiles, Charles D., and David H. Rowitch. 2008. “Glioma Stem Cells: A Midterm Exam.” *Neuron* 58 (6): 832–46. <https://doi.org/10.1016/j.neuron.2008.05.031>.

Stupp, Roger, Warren P. Mason, Martin J. Van Den Bent, Michael Weller, Barbara Fisher, Martin J. B. Taphoorn, Karl Belanger, et al. 2005. “Radiotherapy Plus Concomitant and Adjuvant Temozolomide for Glioblastoma.” *New England Journal of Medicine* 352 (10): 987–96. <https://doi.org/10.1056/NEJMoa043330>.

Sweeney, Eamon. 1995. “Dormant Cells in Columnar Cell Carcinoma of the Thyroid.” *Human Pathology* 26 (6): 691–92. [https://doi.org/10.1016/0046-8177\(95\)90180-9](https://doi.org/10.1016/0046-8177(95)90180-9).

Taipale, Jussi, and Philip A. Beachy. 2001. “The Hedgehog and Wnt Signalling Pathways in Cancer.” *Nature* 411 (6835): 349–54. <https://doi.org/10.1038/35077219>.

Tang, Xuejia, Chenghai Zuo, Pengchao Fang, Guojing Liu, Yongyi Qiu, Yi Huang, and Rongrui Tang. 2021a. “Targeting Glioblastoma Stem Cells: A Review on Biomarkers, Signal Pathways and Targeted Therapy.” *Frontiers in Oncology* 11 (July): 701291. <https://doi.org/10.3389/fonc.2021.701291>.

—. 2021b. “Targeting Glioblastoma Stem Cells: A Review on Biomarkers, Signal Pathways and Targeted Therapy.” *Frontiers in Oncology* 11 (July): 701291. <https://doi.org/10.3389/fonc.2021.701291>.

Turner, C., A. R. Stinchcombe, M. Kohandel, S. Singh, and S. Sivaloganathan. 2009. “Characterization of Brain Cancer Stem Cells: A Mathematical Approach.” *Cell Proliferation* 42 (4): 529–40. <https://doi.org/10.1111/j.1365-2184.2009.00619.x>.

Tzeng, Stephany Y., Hugo Guerrero-Cázares, Elliott E. Martinez, Joel C. Sunshine, Alfredo Quiñones-Hinojosa, and Jordan J. Green. 2011. “Non-Viral Gene Delivery Nanoparticles Based on Poly(beta-Amino Esters) for Treatment of Glioblastoma.” *Biomaterials* 32 (23): 5402–10. <https://doi.org/10.1016/j.biomaterials.2011.04.016>.

Vlashi, Erina, Kwanghee Kim, Chann Lagadec, Lorenza Della Donna, John Tyson McDonald, Mansoureh Eghbali, James W. Sayre, Enrico Stefani, William McBride, and Frank Pajonk. 2009. “In Vivo Imaging, Tracking, and Targeting of Cancer Stem Cells.” *JNCI: Journal of the National Cancer Institute* 101 (5): 350–59. <https://doi.org/10.1093/jnci/djn509>.

Wang, Hanwen, Oleg Milberg, Imke H. Bartelink, Paolo Vicini, Bing Wang, Rajesh Narwal, Lorin Roskos, Cesar A. Santa-Maria, and Aleksander S. Popel. 2019. “*In Silico* Simulation of a Clinical Trial with Anti-CTLA-4 and Anti-PD-L1 Immunotherapies in Metastatic Breast Cancer Using a Systems Pharmacology Model.” *Royal Society Open Science* 6 (5): 190366. <https://doi.org/10.1098/rsos.190366>.

Wang, Hanwen, Richard J. Sové, Mohammad Jafarnejad, Sondra Rahmeh, Elizabeth M. Jaffee, Vered Stearns, Evanthisia T. Roussos Torres, Roisin M. Connolly, and Aleksander S. Popel. 2020. "Conducting a Virtual Clinical Trial in HER2-Negative Breast Cancer Using a Quantitative Systems Pharmacology Model with an Epigenetic Modulator and Immune Checkpoint Inhibitors." *Frontiers in Bioengineering and Biotechnology* 8 (February). <https://doi.org/10.3389/fbioe.2020.00141>.

Weiss, Lora D., Natalia L. Komarova, and Ignacio A. Rodriguez-Brenes. 2017. "Mathematical Modeling of Normal and Cancer Stem Cells." *Current Stem Cell Reports* 3 (3): 232–39. <https://doi.org/10.1007/s40778-017-0094-4>.

Weller, Michael, Nicholas Butowski, David D Tran, Lawrence D Recht, Michael Lim, Hal Hirte, Lynn Ashby, et al. 2017. "Rindopepimut with Temozolomide for Patients with Newly Diagnosed, EGFRvIII-Expressing Glioblastoma (ACT IV): A Randomised, Double-Blind, International Phase 3 Trial." *The Lancet Oncology* 18 (10): 1373–85. [https://doi.org/10.1016/S1470-2045\(17\)30517-X](https://doi.org/10.1016/S1470-2045(17)30517-X).

Wu, Chengyue, Guillermo Lorenzo, David A. Hormuth, Ernesto A. B. F. Lima, Kalina P. Slavkova, Julie C. DiCarlo, John Virostko, et al. 2022. "Integrating Mechanism-Based Modeling with Biomedical Imaging to Build Practical Digital Twins for Clinical Oncology." *Biophysics Reviews* 3 (2). <https://doi.org/10.1063/5.0086789>.

Yan, Min, and Quentin Liu. 2016. "Differentiation Therapy: A Promising Strategy for Cancer Treatment." *Chinese Journal of Cancer* 35 (1): 3. <https://doi.org/10.1186/s40880-015-0059-x>.

Yang, Wei, Nicole M. Warrington, Sara J. Taylor, Paula Whitmire, Eduardo Carrasco, Kyle W. Singleton, Ningying Wu, et al. 2019. "Sex Differences in GBM Revealed by Analysis of Patient Imaging, Transcriptome, and Survival Data." *Science Translational Medicine* 11 (473): eaao5253. <https://doi.org/10.1126/scitranslmed.aao5253>.

Yankeelev, Thomas E., David A. Hormuth, Ernesto A. B. F. Lima, Guillermo Lorenzo, Chengyue Wu, Lois C. Okereke, Gaiane M. Rauch, Aradhana M. Venkatesan, and Caroline Chung. 2024. "Designing Clinical Trials for Patients Who Are Not Average." *iScience* 27 (1): 108589. <https://doi.org/10.1016/j.isci.2023.108589>.

Youssefpour, H., X. Li, A. D. Lander, and J. S. Lowengrub. 2012. "Multispecies Model of Cell Lineages and Feedback Control in Solid Tumors." *Journal of Theoretical Biology* 304 (July): 39–59. <https://doi.org/10.1016/j.jtbi.2012.02.030>.

Yu, Victoria Y., Dan Nguyen, Frank Pajonk, Patrick Kupelian, Tania Kaprealian, Michael Selch, Daniel A. Low, and Ke Sheng. 2015. "Incorporating Cancer Stem Cells in Radiation Therapy Treatment Response Modeling and the Implication in Glioblastoma Multiforme Treatment Resistance." *International Journal of Radiation Oncology*Biology*Physics* 91 (4): 866–75. <https://doi.org/10.1016/j.ijrobp.2014.12.004>.

Zahid, Mohammad U., Abdallah S. R. Mohamed, Jimmy J. Caudell, Louis B. Harrison, Clifton D. Fuller, Eduardo G. Moros, and Heiko Enderling. 2021. "Dynamics-Adapted Radiotherapy Dose (DARD) for Head and Neck Cancer Radiotherapy Dose Personalization." *Journal of Personalized Medicine* 11 (11): 1124. <https://doi.org/10.3390/jpm11111124>.